Climate response to large, high-latitude and low-latitude volcanic eruptions in the Community Climate System Model

David P. Schneider,[1] Caspar M. Ammann,[1] Bette L. Otto-Bliesner,[1] and Darrell S. Kaufman[2]

Received 30 September 2008; revised 7 May 2009; accepted 12 May 2009; published 1 August 2009.

[1] Explosive volcanism is known to be a leading natural cause of climate change. The second half of the 13th century was likely the most volcanically perturbed half-century of the last 2000 years, although none of the major 13th century eruptions have been clearly attributed to specific volcanoes. This period was in general a time of transition from the relatively warm Medieval period to the colder Little Ice Age, but available proxy records are insufficient on their own to clearly assess whether this transition is associated with volcanism. This context motivates our investigation of the climate system sensitivity to high- and low-latitude volcanism using the fully coupled NCAR Community Climate System Model (CCSM3). We evaluate two sets of ensemble simulations, each containing four volcanic pulses, with the first set representing them as a sequence of tropical eruptions and the second representing eruptions occurring in the mid-high latitudes of both the Northern and Southern hemispheres. The short-term, direct radiative impacts of tropical and high-latitude eruptions include significant cooling over the continents in summer and cooling over regions of increased sea-ice concentration in Northern Hemisphere (NH) winter. A main dynamical impact of moderate tropical eruptions is a winter warming pattern across northern Eurasia. Furthermore, both ensembles show significant reductions in global precipitation, especially in the summer monsoon regions. The most important long-term impact is the cooling of the high-latitude NH produced by multiple tropical eruptions, suggesting that positive feedbacks associated with ice and snow cover could lead to long-term climate cooling in the Arctic.

Citation: Schneider, D. P., C. M. Ammann, B. L. Otto-Bliesner, and D. S. Kaufman (2009), Climate response to large, high-latitude and low-latitude volcanic eruptions in the Community Climate System Model, *J. Geophys. Res.*, *114*, D15101, doi:10.1029/2008JD011222.

1. Introduction

[2] Large, explosive volcanic eruptions are known to be a leading cause of natural climate change on a range of timescales. The most important mechanism by which volcanic eruptions perturb climate is the injection of large amounts of SO_2 gas into the stratosphere [e.g., *Robock*, 2000]. The SO_2 reacts with OH and H_2O to form H_2SO_4 + H_2O aerosols, which interact with the incoming and outgoing radiation. Some incoming solar radiation is scattered back to space, leading to cooling at the Earth's surface, while the aerosols also absorb solar near-infrared and terrestrial radiation, leading to lower stratospheric warming inside the aerosol layers.

[3] The most recent large eruption, Pinatubo in 1991, injected an estimated 20Mt of SO_2 into the atmosphere, leading to a temporary ($\sim$2 years) reversal of the late twentieth century global warming trend [*Robock*, 2000]. In many respects, the forcing pattern and response to volcanic aerosols is opposite that of anthropogenic CO_2, which has led some authors to discuss the artificial injection of sulfate into the stratosphere as a means of counteracting antropogenically driven warming [e.g., *Wigley*, 2006; *Crutzen*, 2006; *Rasch et al.*, 2008]. However, there may be adverse impacts associated with aerosol injection, including the significant reduction of tropical precipitation [*Trenberth and Dai*, 2007; *Bala et al.*, 2008] and increased destruction of stratospheric ozone [e.g., *Robock et al.*, 2008; *Tilmes et al.*, 2008].

[4] In the context of the last millennium, volcanic eruptions and solar variability are the two leading natural causes of forced climate variability, and together these factors explain much of the decadal to centennial-scale variance of reconstructed Northern Hemisphere (NH) surface temperatures [e.g., *Crowley*, 2000; *Ammann et al.*, 2007]. Volcanic eruptions have been implicated in droughts, famines, waves of pestilence, and the triggering of centuries-long cold periods [*Stothers*, 2000; *Oman et al.*, 2006a; *Anderson et al.*, 2008]. However, an estimate of the radiative and

[1] Climate and Global Dynamics Division, National Center for Atmospheric Research, Boulder, Colorado, USA.
[2] Department of Geology, Northern Arizona University, Flagstaff, Arizona, USA.

0148-0227/09/2008JD011222

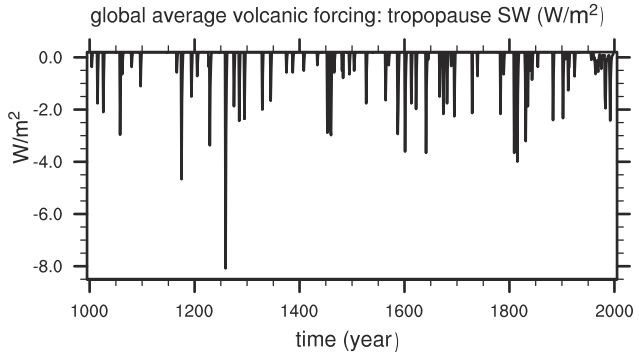

Figure 1. Global average, annual mean volcanic forcing for the years 1000–2000 AD, as compiled by the IPCC Fourth Assessment Report and originally by *Crowley* [2000]. Data were obtained from the World Data Center for Paleoclimatology, Boulder, Colorado.

dynamical forcing associated with an eruption requires knowledge of the latitude and size of an eruption, information that is generally not directly available from historical records or proxies. At the same time, estimating the response requires a large number of spatially distributed climate proxy data, and the number of suitable records decreases back in time. Much uncertainty remains in the estimation of surface temperatures, and forcing factors, especially before about 1600 AD [*National Research Council*, 2006].

[5] In both the modern context and the past 1000 years, better understanding of volcanic impacts on climate requires evaluation of both the radiative and dynamic effects of stratospheric sulfate aerosols, which can originate from volcanic eruptions at high or low latitudes [*Robock*, 2000], or in theory from artificial injection [*Crutzen*, 2006]. Coupled climate system models are particularly useful tools for addressing this problem. Climate models have been successfully employed to simulate the major observed effects of large volcanic eruptions [*Graf et al.*, 1993; *Kirchner et al.*, 1999; *Shindell et al.*, 2001; *Stenchikov et al.*, 2002, 2004], although straightforward evaluation is often limited by the number of observations, the method of incorporating volcanic forcing into the model, and the problem of separating internal variability with comparable impacts such as El Niño from volcanic signals [*Robock*, 2000].

[6] Here we describe a series of experiments that were conducted with a current generation, fully coupled atmosphere-ocean general circulation model. We present two scenarios for the period 1250–1300AD, likely the most volcanically perturbed half-century of the last millennium, as indicated in the IPCC AR4 Chapter 6 [*Jansen et al.*, 2007], and reproduced in Figure 1. Our simulations facilitate the direct comparison of the impacts of tropical and high-latitude eruptions, the consideration of the long-term effects of closely sequenced eruptions, and comparison of the responses to events of different magnitudes. Four large events occurred at 1257–58, 1269, 1278 and 1286. In the IPCC interpretation, all of these events are implicitly assumed to be tropical in origin, yet there are several questions about this period as discussed below. A new synthesis of ice core records of volcanism [*Gao et al.*, 2008] agrees well with the IPCC figure. In both studies, 1257–58 is by far the largest signal in both hemispheres and globally for the period from 500 AD to 2000 AD. In terms of total sulfate aerosol injection, the *Gao et al.* [2008] compilation indicates that 1278 and 1286 were roughly twice as large as Pinatubo. These events make the sulfate loading in the 13th century two to ten times larger than any other century in the last 1500 years [*Gao et al.*, 2008].

[7] Tropical eruptions are widely believed to have the greatest climate impact (compared to a high-latitude eruption) because the stratospheric aerosol cloud covers a large surface area, has a longer residence time, and is transported poleward in both hemispheres, eventually covering the entire globe. Evidence for tropical eruptions during the 1250–1300 period is the presence of large spikes in non-sea-salt-sulfate concentration in polar ice cores from Greenland and Antarctica [*Langway et al.*, 1995; *Oppenheimer*, 2003; *Gao et al.*, 2008]. However, none of these eruptions have been directly attributed to specific source volcanoes through geochemical fingerprinting or historical record matches. An original study on the apparently massive 1257–58 event [*Palais et al.*, 1992], for instance, proposed the relatively sulfur-rich El Chichón volcano, but this interpretation was later questioned [*Oppenheimer*, 2003; *Kurbatov et al.*, 2006]. Moreover, annually resolved NH temperature reconstructions [e.g., *Jansen et al.*, 2007] and tree ring records [*D'Arrigo et al.*, 2001, 2006] show no remarkable climate anomaly in the 1250s, as would be expected for huge (~200 Mt peak aerosol mass) tropical events. One possibility is that tree growth may be enhanced after eruptions because of enhanced diffuse radiation [*Robock*, 2005]. Nonetheless, in other notable volcanically perturbed periods, such as 1600–1650 and 1800–1850 AD, temperature reconstructions show strong evidence for volcanically forced cooling in the particular years in question, but there still may have been more cooling at these times than suggested by tree ring based reconstructions [*Robock*, 2005].

[8] A recent review by *Oppenheimer* [2003] cites some climatic anomalies roughly consistent with the timing of the 1258 event, yet they are weaker than the forcing would suggest. Others have hypothesized that the aerosol size distribution may have been different than for other historic eruptions, such that the global radiation budget would have been affected less than otherwise assumed [*Crowley and Kim*, 1999; *Hyde and Crowley*, 2000; *Lorenz et al.*, 2008]. In some regions of the NH, principally around the North Atlantic, there is evidence for glacial advances in the 13th century and by inference, cooling [*Grove*, 2001; *Anderson et al.*, 2008]. Moreover, new assimilations of proxy data from lake sediments, ice cores, and tree rings indicate cooling across the Arctic at this time [*Crespin et al.*, 2009; *Kaufman*, 2009], suggesting that any long-term volcanic impacts may have been confined to the NH high latitudes. Some authors interpret this period as the onset of the "Little Ice Age" [*Grove*, 2001], and it was in general a time of transition from the relatively warm Medieval period. However, volcanic signals may be superimposed on top of high-latitude cooling during the late Holocene associated with orbital forcing [e.g., *Kaufman et al.*, 2004; *Wanner et al.*, 2008], complicating their identification. *Stothers* [2000] reviews evidence for the impacts of the 1258 event, citing large and adverse effects on crops, famine and disease in Europe. If not tropical in origin, a

plausible alternative forcing scenario for this time period is that multiple eruptions occurred at high latitudes in both hemispheres. In the NH, there are numerous candidates for 13th century volcanism, including volcanoes in Iceland and the Aleutian islands. In the Southern Hemisphere (SH), candidate volcanoes include several in southern South America and Mt. Melbourne in Antarctica [*Kurbatov et al.*, 2006].

[9] Our two scenarios for the period 1250–1300 AD are a tropical volcanism case and a high-latitude volcanism case. Both cases are constrained by the ice core sulfate records, as either forcing scenario could explain the sulfate concentrations found in ice cores in both polar regions. We evaluate and compare two sets of 50-yearlong ensembles, the first representing a sequence of four tropical eruptions, and the second representing identically sequenced eruptions occurring in the mid to high latitudes of both the Northern and Southern hemispheres.

[10] Motivated by the late 13th century volcanic and climate records, this study builds upon previous model-based studies of volcanism and climate in a few key ways. Most studies have used atmosphere-only models with fixed climatological sea surface temperatures (SSTs) and sea-ice extent [*Robock and Liu*, 1994; *Stenchikov et al.*, 1998, 2002, 2004; *Kirchner et al.*, 1999; *Oman et al.*, 2005], a mixed-layer ocean [*Shindell et al.*, 2001, 2003], a mixed-layer ocean and dynamic only sea ice [*Oman et al.*, 2006a], or other simplified setups [e.g., *Graf et al.*, 1993]. These representations may miss some aspects of the full dynamical response to volcanic eruptions, particularly those feedbacks that can lead to long-term climate change. For instance, in the Northern Hemisphere, a focus of this study, sea ice and ocean circulation are two of the major climate system components. Winter sea ice shows significant anomalies associated with the Northern Annular Mode [*Rigor et al.*, 2002], which itself is known to respond to volcanic eruptions [e.g., *Robock*, 2000; *Shindell et al.*, 2004; *Kirchner et al.*, 1999]. Summer sea-ice extent is also associated with atmospheric circulation anomalies [*Ogi and Wallace*, 2007]. Here we use a fully coupled climate system model that allows the full climate system response to volcanic eruptions to be examined. The few previous studies of the volcanic forcing in coupled models [*Stenchikov et al.*, 2006; *Ammann et al.*, 2007] have largely evaluated transient simulations, which include a variety of other time-varying forcings (solar, anthropogenic), making the volcanic signal difficult to isolate. Our experimental design is a sensitivity test with strong volcanic aerosol forcing with other forcings held constant, permitting straightforward signal detection. Finally, most studies have focused on tropical [*Kirchner et al.*, 1999; *Robock*, 2000; *Stenchikov et al.*, 2002, 2004] or high-latitude [*Oman et al.*, 2006a, 2006b] events in isolation, but not a systematic comparison of both in similarly designed experiments.

[11] The remainder of this paper is organized as follows. In section 2, we describe the model, experimental setup, forcing data set, and calculation of the radiative perturbation. In section 3, we present the key results of our simulations. We focus primarily on NH surface climate, in part because it shows the largest response, and in part because the majority of available observational and climate proxy data are from the NH. For surface climate, we focus on anomalies in temperature, winds, sea level pressure, sea-ice concentration and precipitation. We also consider the dynamical response through examination of vertical profiles in zonal wind and temperature anomalies. Section 4 provides discussion and conclusions of our study.

2. Model and Forcing Description

[12] We use the Community Climate System Model, Version 3 (CCSM3), a global climate model with coupled atmosphere, ocean, sea ice and land components, jointly developed by the National Center for Atmospheric Research and community partners. An overview of the model is provided by *Collins et al* [2006]. The coupled model has been used extensively to simulate the climate of the 20th century [*Meehl et al.*, 2006], climate change projections for the 21st century [*Meehl et al.*, 2006], as well as for paleoclimate studies [e.g., *Otto-Bliesner et al.*, 2006b]. Of specific interest for this study are the model's representations of atmospheric variability [*Alexander et al.*, 2006; *Hurrell et al.*, 2006], sea ice [*DeWeaver and Bitz*, 2006; *Holland et al.*, 2006a], and preindustrial climate [*Otto-Bliesner et al.*, 2006a]. Although volcanic forcing has been included in 20th century simulations of the CCSM3 [*Meehl et al.*, 2006], in preindustrial simulations with an earlier version of the model [*Ammann et al.*, 2007], and in single forcing simulations with the related Parallel Climate Model [*Ammann et al.*, 2003; *Wigley et al.*, 2005; *Arblaster and Meehl*, 2006], no study has provided a detailed account of the climate response to volcanic eruptions in the CCSM3.

[13] Our simulations with CCSM3 are conducted with a configuration of the atmosphere and land component models on a $2.8^\circ \times 2.8^\circ$ latitude-longitude grid and the ocean and sea-ice models on a roughly $1^\circ \times 1^\circ$ horizontal grid. The atmosphere, with a spectral dynamical core (T42), has 26 levels in the vertical and the ocean has 40 levels [*Collins et al.*, 2006; *Otto-Bliesner et al.*, 2006a]. This configuration is computationally more efficient than the T85 $\times$ 1 used in climate change projection studies [*Meehl et al.*, 2006], making it useful for long and ensemble paleoclimate integrations [e.g., *Otto-Bliesner et al.*, 2006a].

[14] As a control case, we use 50 years of the 400-yearlong, preindustrial simulation described by *Otto-Bliesner et al.* [2006a]. The atmospheric concentrations of greenhouse gasses, aerosols and ozone, as well as the solar constant and orbital year parameters, are chosen to represent average late Holocene conditions (Table 1). Three different January 1st conditions of the control were selected as initial conditions for the three ensemble members of our volcanically perturbed scenarios. For this study, each ensemble member is run for a period of 50 years, corresponding to calendar years 1250–1299 AD. As shown below, the volcanic forcing is quite large, so three ensemble members for each scenario are adequate for isolating the volcanic signal from the background internal variability.

[15] The volcanic forcing for tropical eruptions is that used in the study of *Ammann et al.* [2007]. Peaks in non-sea-salt sulfate concentration occurring simultaneously in ice core records in both polar regions are interpreted as markers of tropical eruptions. The ice core sulfate concentration is converted to time-varying and latitudinally varying stratospheric aerosol load using linear scaling, following previous work [*Ammann et al.*, 2003, 2007] and similarly described by

Table 1. Values of the Forcing Terms Used in the Control and Volcanic Simulations [After *Otto-Bliesner et al.*, 2006a]

CO_2	280 ppm
CH_4	760 ppb
N_2O	270 ppb
O_3	1870 AD
Sulfate aerosols (troposphere)	1870 AD
Dust and sea salt	present-day
Carbonaceous aerosols	30% of present-day
Solar constant	1365 W/m^2
Orbital year	1950 AD

Gao et al. [2008]. The stratospheric aerosols are prescribed in the model as a fixed, single-size distribution, which mimics the average observed characteristics of the Pinatubo aerosol. Gas injection is instantaneous, followed by a gas-to-aerosol conversion over four months. All aerosol is assumed to be well mixed and is applied uniformly in the zonal dimension. Due to the low vertical resolution in the climate model, the aerosol resides in three layers in the lower stratosphere above the tropopause, taking latitudinal changes into account, without evolution of the vertical profile over time. For each tropical eruption, the aerosol cloud originates in the tropics, builds and spreads over a few months before decaying, and is transported poleward six months to a year after the eruption [*Ammann et al.*, 2003]. As an example, we show the aerosol optical depth for the 1258 event (Figure 2a).

[16] The volcanic aerosol for the high-latitude eruptions is assumed to have the same size distribution characteristics as the tropical volcanic aerosol, but the aerosol cloud is limited to latitudes poleward of 30° in each hemisphere, as stratospheric transport is predominantly poleward (Figure 2b). There is no example of significant cross-equator transport of aerosols for a high-latitude eruption. For instance, observations indicate that the aerosol cloud from the 1912 Katmai eruption in Alaska was clearly restricted to north of 30°N [*Stothers*, 1996].

[17] The timing of the high-latitude volcanic eruptions is adjusted by a few months relative to the tropical eruptions to match the arrival time of the aerosol clouds over the ice core sites. To explain the same sulfate signal in a polar ice core record, high-latitude eruptions must occur later than tropical eruptions. Also, the required total aerosol mass is lower for high-latitude eruptions than for tropical eruptions because of the shorter transport distance and a smaller area of removal. Table 2 compares the estimated peak aerosol mass and timing for high-latitude and tropical eruptions. To achieve a comparable polar sulfate flux to a tropical eruption, the contemporaneous high-latitude eruptions inject only about two thirds of the peak aerosol mass of the tropical eruptions. In Figure 2, we compare the zonal mean optical depth for the 1258 event for the high-latitude scenario versus the tropical-forcing scenario. The tropical aerosol covers a much larger area over a slightly longer period of time. High-latitude aerosols are removed from the stratosphere relatively quickly because of strong subsidence in the polar vortex. The other events evolve similarly to the 1258 event, although 1258 is by far the largest. These patterns of zonal mean optical depth qualitatively agree well with calculations by other models [e.g., *Oman et al.*, 2005, 2006a; *Ammann et al.*, 2003] and with observations [e.g., *Stenchikov et al.*, 1998].

[18] Given the prescribed aerosol loads, the climate model calculates the radiative perturbation for each event (Figure 3). The change in global average surface shortwave (SW) radiation for the 1258 tropical case quickly reaches -24 W m^{-2} in January, 1258, about four months from the start of the eruption (Figure 3a). The pertubation decays more slowly than it grew, lasting for about three years until the beginning of 1261. The three subsequent events are smaller than the 1258 event, but each is associated with a larger surface shortwave perturbation than the observed -4 W m^{-2} peak forcing associated with the 1991 Pinatubo eruption [*Stenchikov et al.*, 1998]. The 1258 high-latitude case has a significant global average shortwave perturbation of -8 W m^{-2}, although the lifetime is well under three years due to the direct removal of aerosols at high latitudes [*Ammann et al.*, 2003; Figure 3b]. In comparison to a well-known high-latitude eruption scenario with a different model, *Oman et al* [2006b] computed a global mean forcing of slightly less than -4 W m^{-2} for the 1783 Laki eruption. Our high-latitude scenario includes eruptions in both hemispheres, and thus the NH forcing is broadly similar to the *Oman et al.* [2006b] Laki simulation.

[19] Although tropical eruptions produce a larger global average change in shortwave radiation, high-latitude eruptions produce larger changes in peak forcing in the NH extratropics (40°–90°N; Figures 3c–3d). Examining the

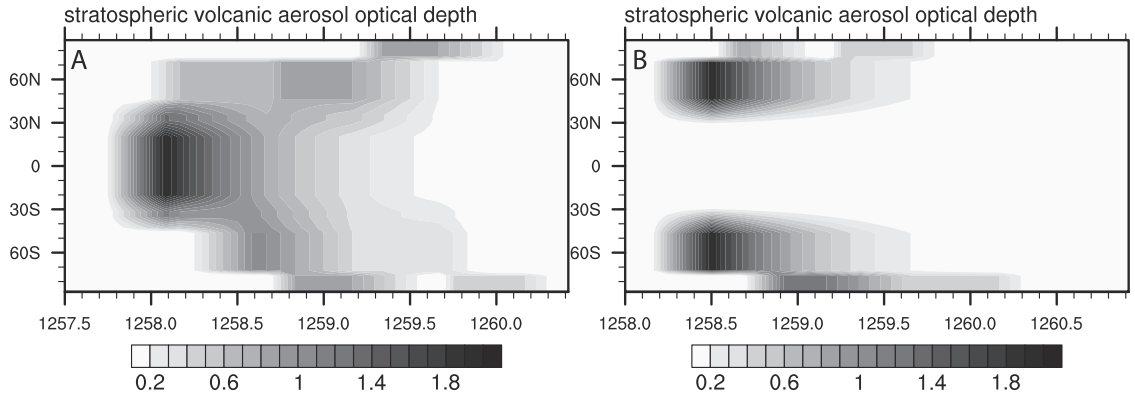

Figure 2. Offline modeled zonal mean optical depth from stratospheric aerosols for the unknown ~1258 AD volcanic eruption, assuming either (a) a single large eruption at the equator or (b) an eruption at about 50° latitude in the Northern and Southern hemispheres.

Table 2. Dates (AD) of Simulated Eruptions and the Peak Aerosol Mass (Mt)

	Tropical Eruption Date	Tropical Eruption Peak Aerosol Mass	High-Latitude Eruptions Date	High-Latitude Eruptions Peak Aerosol Mass
Event 1	October 1257	200	April 1258	124
Event 2	January 1269	40	May 1269	25
Event 3	January 1278	75	March 1278	47
Event 4	April 1286	40	July 1286	25

1258 event in more detail (Figures 3e–3f), further differences of the two forcing scenarios are apparent. For the tropical eruption case (Figure 3e), the global average reaches its maximum in early 1258 and declines thereafter. Meanwhile, as the global average shortwave perturbation decreases, the extratropical forcing increases. The extratropical perturbations are clearly in phase with the seasonal cycle, with the largest effects in summer and the smallest in winter. However, the extratropics receive limited solar radiation in the winter, so the absolute changes in shortwave radiation are

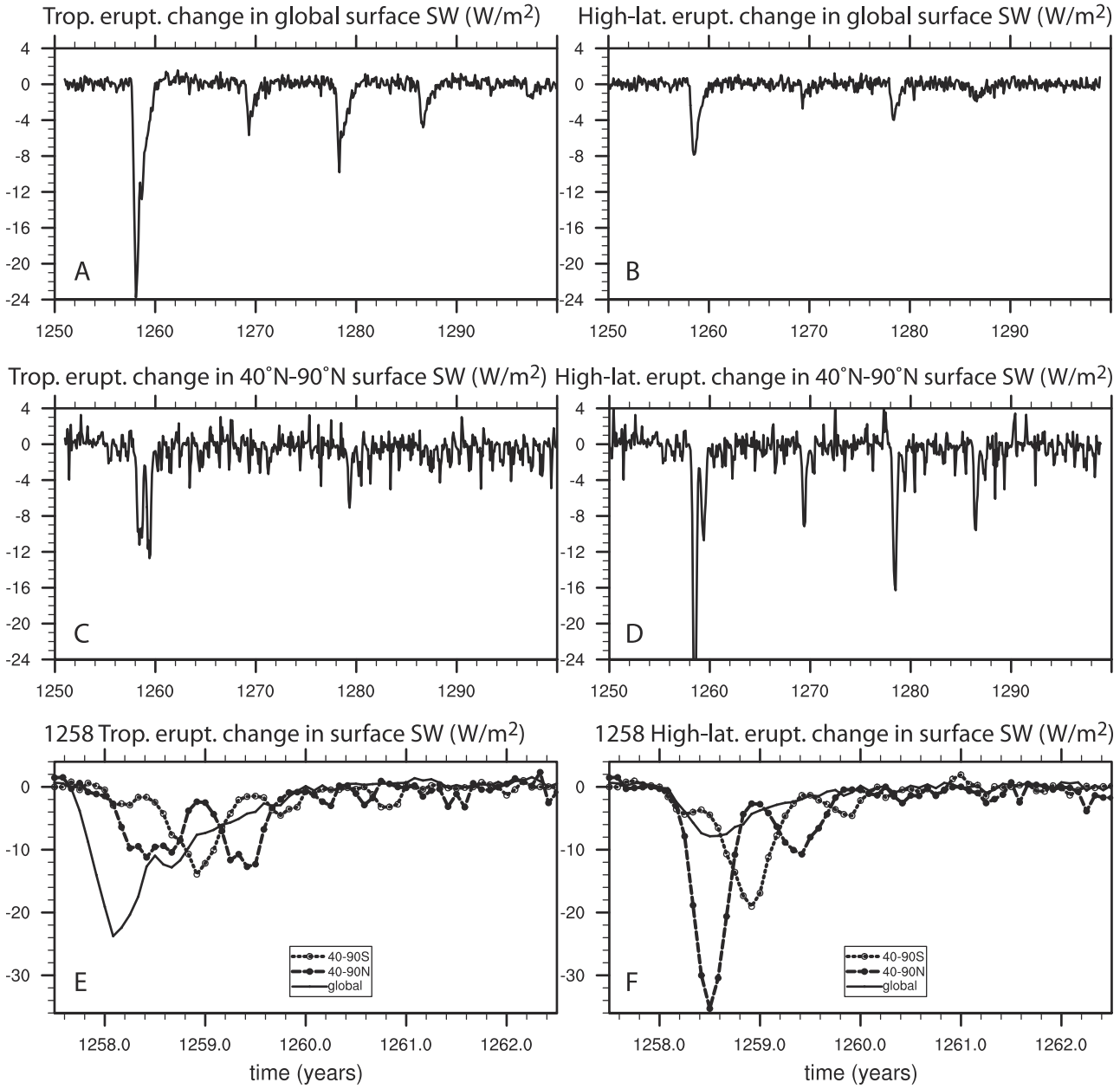

Figure 3. Changes in monthly average shortwave radiation at (left) the surface for the tropical eruption scenario and (right) the high-latitude scenario computed by the CCSM3: (a and b) for the global mean, (c and d) for the NH poleward of 40° N, (e and f) for the 1258 event only. Solid line, global mean; solid circles, NH poleward of 40° N; open circles, SH poleward of 40° S.

significant. The NH perturbations of about -12 W m^{-2} peak in the summer months of 1258 and again during the summer of 1259. Smaller perturbations occur in 1260 and 1261. The winter NH extratropics experience a shortwave perturbation on the order of -2 to -3 W m^{-2}. The SH experiences a very large perturbation, about -14 W m^{-2}, only for one summer season.

[20] For the high-latitude case (Figure 3f), the time evolution of the global average shortwave anomaly more closely follows that of the extratropics. The largest perturbation of -36 W m^{-2} occurs in the NH extratropics in the summer of 1258, similar in timing but different in magnitude to the tropical-forcing scenario. A second large perturbation, of about -12 W m^{-2}, in the NH occurs in the summer of 1259, similar in size and timing to the perturbation for the tropical case. For the high-latitude case, the SH extratropics experience a very large surface shortwave perturbation of -20 W m^{-2} in one summer, 1258–59. The radiative perturbations for each of the other three events evolve qualitatively similarly to the 1258 event, varying according to the differences in the magnitude of the event and its timing in the seasonal cycle.

[21] Overall, for the 1258 event, the monthly peak forcing is about 50–60% larger than the values suggested by *Crowley* [2000]. An important difference in *Crowley's* [2000] approach to estimate radiative forcing was the additional application of a forcing dampening factor motivated by an apparently limited climate impact recorded in proxy records and supported by possible evolution of the particle sizes [*Pinto et al.*, 1989] reducing aerosol forcing by the 2/3 power for very large events. Our volcanic aerosol implementation does not directly apply a specified radiative forcing, but rather computes the radiative effect of a specified mass of aerosol (assuming a fixed size distribution, see above). Our experiments, therefore, test more dynamically whether the period might better be explained by multiple high-latitude eruptions, rather than assuming changes to the size distribution of aerosols for very large events. The next generation of the CCSM is expected to implement particle size evolution, which will enable experiments that explicitly test these assumptions about the forcing for very large volcanic events.

[22] It should be noted that our specific model configuration and preindustrial scenarios might exaggerate some aspects of the response to volcanic eruptions and weaken other aspects in comparison to present-day observations. The global average surface temperature in the preindustrial control climate simulation is 1.3°C cooler than the present-day, while the high latitudes of the NH (poleward of ~75°N) are cooler by 4°C or more. The sea ice is thicker in the Arctic basin in all seasons, while in the winter season, relatively thin ice extends southward into the Labrador Sea in the Atlantic and from the Bering Sea to northern Japan in the Pacific [*Otto-Bliesner et al.*, 2006a]. While the thicker ice likely makes the central Arctic less responsive to subtle changes in forcing than present-day ice, the colder preindustrial climate likely promotes more ice growth in the marginal seas (e.g., Labrador, Bering), regions where ice thickness and extent is overestimated in present-day model configurations [e.g., *Holland et al.*, 2006a].

[23] Another important mechanism in the response to volcanic eruptions involves the equator-pole stratospheric temperature gradient. In the present day, this gradient can be changed by stratospheric ozone depletion, which tends to increase with the presence of volcanic sulfate aerosols, leading to polar stratospheric cooling [e.g., *Solomon*, 1999; *Robock*, 2000; *Stenchikov et al.*, 2002; *Tilmes et al.*, 2008]. In the absence of anthropogenic chlorine in the stratosphere, ozone depletion is believed to be largely absent in the preindustrial climate, and stratospheric ozone may even increase slightly after volcanic eruptions [*Solomon*, 1999]. Volcanic eruptions emit HCl, but it is efficiently removed by precipitation, so volcanic eruptions are not a significant source of stratospheric chlorine [*Solomon*, 1999]. Changes to stratospheric ozone are not included in our model configuration.

[24] A further consideration is the model itself, as the atmospheric component of the CCSM3 does not have a vertically high-resolution stratosphere and its model top is at 2.2 hPA, though the lower stratosphere-upper troposphere region is more refined than in previous versions of the model [*Hack et al.*, 2006]. The stratospheric configuration may bias the model's dynamical response, as suggested by *Stenchikov et al.* [2006]. The response of the winter 50-hPA height in the polar region to volcanic eruptions in the CCSM3 is comparable to other models, but is (like in the other models) weaker than observations [*Stenchikov et al.*, 2006]. Also, the polar vortex in the models does not respond as strongly to volcanic eruptions as suggested by observational studies, and the typically observed winter warming pattern over Europe and Asia is not as strong in models [*Stenchikov et al.*, 2006]. However, a model's surface temperature response is not solely determined by its stratospheric heating or cooling [*Stenchikov et al.*, 2006], possibly because the surface boundary conditions (SST, sea ice, albedo) and subtleties in the models' stratosphere-troposphere coupling also determine the response [e.g., *Shindell et al.*, 2004]. As we show below, most aspects of the response are robust across a range of models and background climate states, including global surface cooling, stratospheric warming, and widespread changes in precipitation and atmospheric circulation. In addition, we show that the type of volcanic eruption, whether a large tropical eruption like Pinatubo, a potentially much larger tropical eruption like the 1258 event, or a high-latitude eruption, also influences the dynamical response.

3. Results

[25] The response of the climate system in the simulations to the prescribed volcanic forcing is immediate and large. The following results highlight the systematic changes in surface temperature, sea level pressure, precipitation, sea ice, and vertical profiles of atmospheric temperature and zonal winds. For both scenarios, we use the ensemble mean and calculate the anomalies in reference to the climatology of a 50-year period of the control run.

3.1. Surface Temperature

[26] Figure 4 shows the zonally averaged surface temperature anomalies for the NH summer (JJA) and winter (DJF) seasons for all years of both scenarios. The effects of the four volcanic events can be clearly seen. For the tropical case in JJA (Figure 4a), temperatures drop by up to 3°C in the tropics and more than 4°C over the midlatitudes of the NH. Cooling

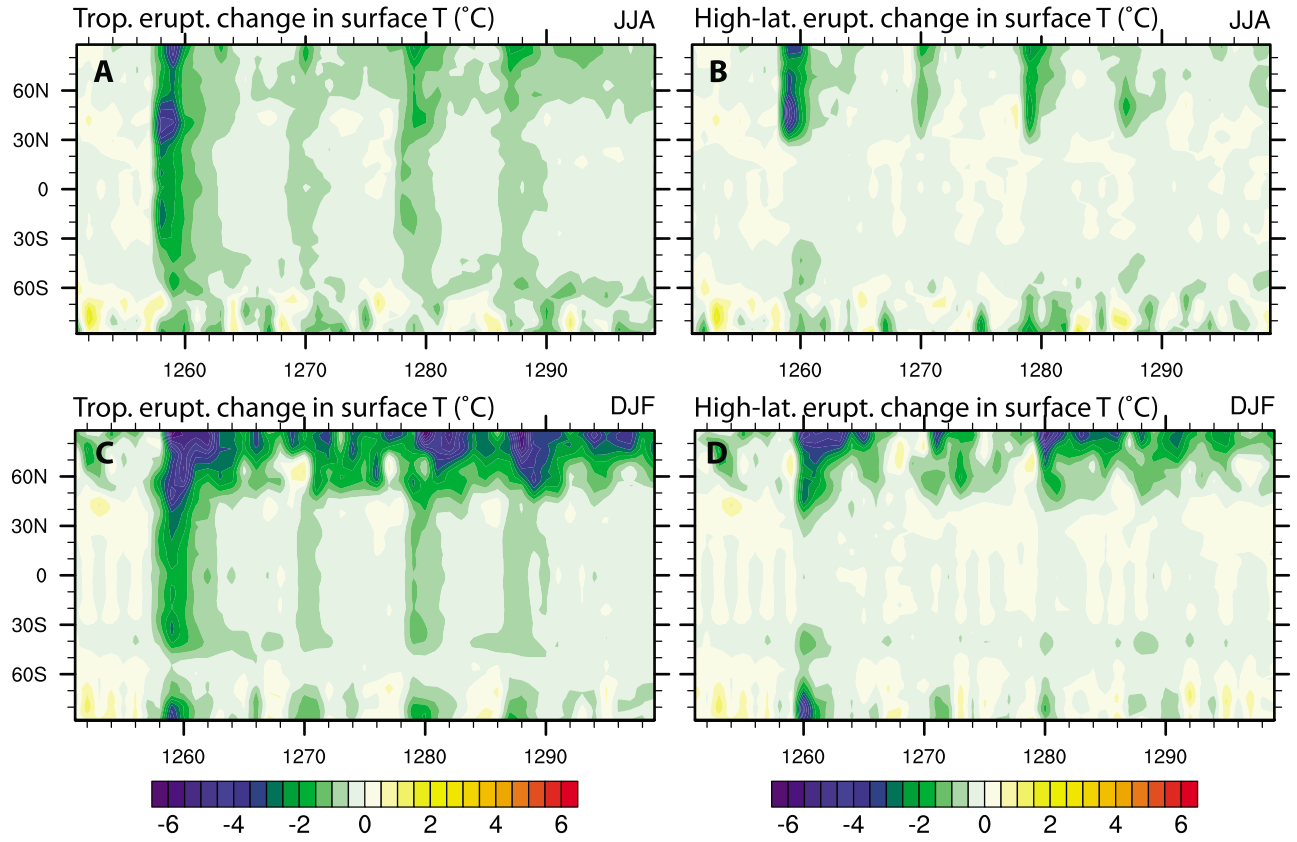

Figure 4. Change in zonal mean, seasonally averaged near-surface temperature for (left) the tropical eruption scenario and (right) the high-latitude scenario. (a) JJA temperatures for tropical eruptions; (b) JJA temperatures for high-latitude eruptions; (c) DJF temperatures for tropical eruptions; (d) DJF temperatures for high-latitude eruptions. The units of the x-axis are years AD.

of up to 1°C persists after the 1258 event until 1262 in the tropics and until 1264 in the NH high latitudes. Anomalies of up to 0.5°C last throughout the entire simulation across all latitudes except the Antarctic. The effects of the high-latitude scenario are less severe (Figure 4b). Cooling of greater than 0.5°C in JJA is restricted to latitudes north of 30°N, and the anomalies are not as persistent as in the tropical scenario. In DJF (Figure 4c), the tropical scenario shows cooling of 4–5°C over latitudes north of 45°N after the events. Cooling of at least 3°C persists throughout the simulation in the NH high latitudes, while the tropical cooling in DJF is similar to the cooling in JJA. The major effects of the high-latitude scenario in DJF (Figure 4d) are mostly restricted to latitudes of aerosol presence, poleward of 30°N and 30°S. Although the forcing is strongest in the summer, it appears that for both forcing scenarios the cooling response is largest and most persistent in the NH winter. This suggests the operation of feedbacks associated with sea ice and/or changes in the atmospheric circulation, which we will discuss further below.

[27] As evident in Figure 4, the 1258 event has much larger impacts on surface temperatures than the other, smaller events. Figure 5 shows the winter season surface air temperature and sea level pressure anomalies for the 1258 tropical event compared with the anomalies composited for the other three tropical events. The composites for the smaller events facilitate (Figures 5b and 5d) a general comparison with the model evaluations presented by *Stenchikov et al.* [2006]. One of the main results is that the smaller events show a winter warming pattern across northern Eurasia that is broadly consistent with observations and previous model simulations [e.g., *Robock*, 2000; *Stenchikov et al.*, 2002, 2004]. However, this winter warming pattern is not found for the 1258 event. The response to the huge 1258 eruption is similar to that found by *Shindell et al.* [2003] in their model study of the 1815 Tambora eruption scaled to twice the size of Pinatubo (2P) and scaled to three tines the size of Pinatubo (3P). While the 2P simulation shows the winter warming pattern, the 3P simulation does not. *Shindell et al.* [2003] conclude that direct radiative forcing dominates the surface temperature changes in the 3P simulation, despite the short-term dynamical changes associated with the winter warming pattern.

[28] Table 3 summarizes the differences in the magnitude of changes in global temperatures, northern Eurasian temperatures, and the NH polar vortex for both the tropical and high-latitude scenarios and separated for the 1258 event versus the composite of the smaller events. Also shown are the results by *Stenchikov et al.* [2006] for the 20th century observations and for an ensemble of 20th century simulations with the CCSM3. The results for the smaller tropical eruptions are consistent with a stronger NH polar vortex, as observed. It is not clear why the simulations analyzed by *Stenchikov et al.* [2006] mostly do not show the winter warming pattern in the right place and a strong polar vortex after 20th century eruptions, which were much weaker than the *Shindell et al.* [2003] simulated 3P and our 1258 event. One possibility is that the 20th century simulations are forced with numerous

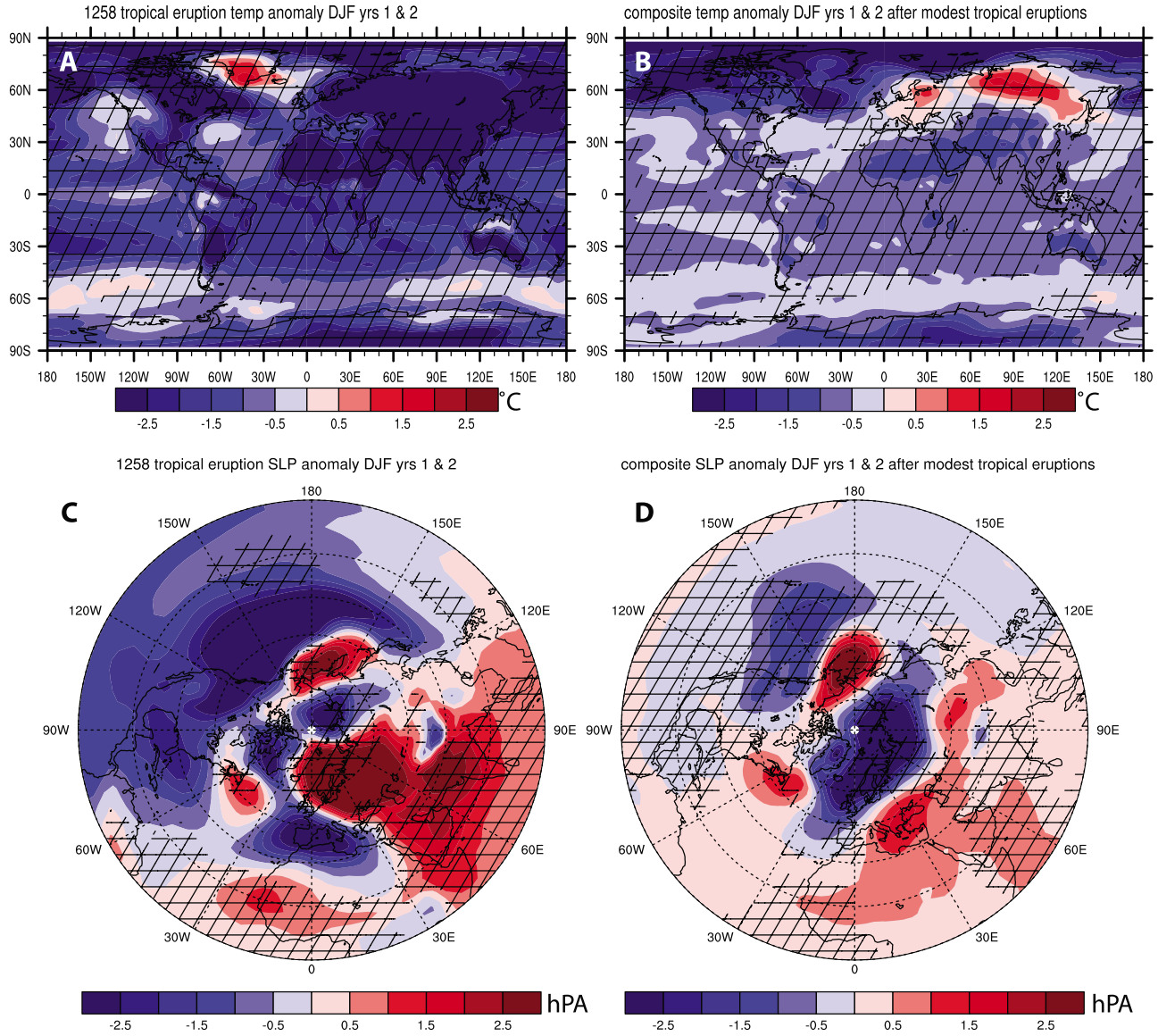

Figure 5. Near-surface air temperature anomalies and SLP anomalies averaged for two winter DJF seasons immediately following tropical eruptions. Compared are (a and c) the anomalies for the very large 1258 event and (b and d) the composite for the smaller 1269, 1278, and 1286 events. Scaling is as by *Stenchikov et al.* [2006]. Anomalies that pass a local Student's *t* test at the 95% level or above are marked with cross-hatching, assuming that each eruption and each model realization are independent samples.

time-varying forcings, not just volcanic aerosols, so it may be rather difficult to completely isolate the volcanic signal, if the other forcings produce large transient responses. In general, most coupled models have difficulty simulating the magnitude of the late 20th century positive trend in the North Atlantic Oscillation (NAO) or Northern Annular Mode [e.g., *Miller et al.*, 2006], a problem which may be related to the same dynamical biases suspected by *Stenchikov et al.* [2006]. *Deser and Phillips* [2009] point out that the CCSM3 may not produce the observed trend in the NAO in part because of discrepancies between the observed evolution of SST and SSTs simulated by the coupled model. Using the stand-alone atmospheric component model, CAM3, *Deser and Phillips* [2009] show that while simulations forced by observed SST and atmospheric radiative forcing produce a positive NAO trend (although only about half as strong as observed), simulations forced with radiative forcing alone and climatological SSTs produce only a very weak NAO response. This again underscores the point that the surface boundary conditions, and not just the stratospheric dynamics, influence the dynamical response seen in the lower troposphere. In the observations, isolating the volcanic signal is also difficult because of interannual to decadal-scale variability associated with large-scale climate phenomena such as the El Niño-Southern Oscillation. In the 20th century period, El Niño events tended to coincide with volcanic eruptions, but similar coincidence of volcanic eruptions and El Niños is not typically found in model simulations [e.g., *Robock*, 2000].

[29] In the following composites we use all four episodes to emphasize the net impacts of all four events in the

Table 3. Integrated Model Responses Averaged Over 1 and 2 Winter Seasons Following Volcanic Eruptions[a]

Simulation, Composite	SAT GL, K	Tropical SAT, K	Arctic SAT, K	SAT ES, K	Tropical T 50, K	Arctic T 50, K	Arctic Z 50, m	Arctic SLP, hPA
Tropical ensemble, 1269, 1278, 1286 events (2 seasons)	−0.71	−0.69	−2.04	0.29	2.1	−0.81	−104	−1.85
Tropical ensemble, 1258 event (2 seasons)	−1.76	−1.91	−2.07	−4.01	10.3	−0.81	48.4	−0.03
High-latitude ensemble, 1269, 1278, 1286 events (2 seasons)	−0.36	−0.07	−1.79	−0.43	0.16	0.46	−28.9	−0.98
High-latitude ensemble, 1258 event (2 seasons)	−0.97	−0.43	−3.16	−1.99	0.51	0.46	80.7	−0.16
CCSM3 20th century, as analyzed by *Stenchikov et al.* [2006]	−0.13	–	–	−0.32	1.32	–	−31	0.1
20th century observations, *Stenchikov et al.* [2006]	0.03	–	–	1.28	1.25	–	−134	−1.98
Tropical ensemble, 1269, 1278, 1286 events (1 season)	−0.47	−0.45	−1.76	0.73	1.65	−1.22	−111	−2.23
Tropical ensemble, 1258 event (1 season)	−1.12	−1.46	−0.48	−3.17	13.8	0.71	−28.4	−1.24
High-latitude ensemble, 1269, 1278, 1286 events (1 season)	−0.38	0.02	−2.23	−0.34	0.25	0.89	−32.4	−1.38
High-latitude ensemble, 1258 event (1 season)	−1.15	−0.5	−2.96	−2.35	1.23	3.08	−32.4	0.6

[a]Abbreviations: SAT GL, global average surface air temperature (SAT); tropical SAT, SAT averaged over 0°–30°N; Arctic SAT, SAT averaged over 65°–90°N; SAT ES, SAT averaged over Eurasia, 30°–130°E, 45°–70°N; Tropical T50, temperature at 50 hPA averaged over 0°–30°N; Arctic T50, temperature at 50 hPA averaged over 65°–90°N; Arctic Z50, geopotential height at 50 hPA averaged over 65°–90°N; Arctic SLP, sea level pressure averaged over 65°–90°N.

simulations, and to highlight the differences in the climate response to tropical versus high-latitude eruptions. The 1258 event is dominant in the tropical composites. Figure 6 shows the surface air temperature anomalies composited for the four volcanic episodes for the first (''season 1'') and second (''season 2'') winter or summer seasons after the eruptions. The temperature response is not zonally symmetric. For the tropical scenario in JJA (Figure 6a), the largest cooling first occurs over the tropical land masses. This pattern can be explained by the reduction of shortwave radiation reaching the surface under the dense aerosol cloud, and by the lower heat capacity of the land compared with the ocean. By season 2 (Figure 6b), the tropical cooling remains significant while the large surface temperature anomalies spread poleward in both hemispheres. This strengthening and poleward spreading of the anomalies can to first order be explained by the long lifetime of aerosols in the tropical stratosphere and by their poleward transport. In contrast, the high-latitude forcing scenario produces the greatest anomalies over the NH continents in season 1 (Figure 6c), and the anomalies decrease in magnitude and significance by season 2 as the forcing is reduced (Figure 6d). The SH high-latitude eruption appears to have a relatively small impact on SH climate. Interestingly, there is a small warming of about 1°C over eastern India, the Arabian Peninsula and the Sahel region of Africa, just south of the edge of the aerosol cloud. As we will show below, the warming pattern is associated with reduced monsoon circulations and a decrease in tropical precipitation. *Oman et al.* [2006a], in their study of the climatic impacts of the 1783 Laki eruption in Iceland, claim that reduced precipitation in the monsoon regions is the main dynamical impact of high-latitude eruptions. Our results support this claim, suggesting that this pattern is a main response of the climate system to large high-latitude eruptions and not a model-dependent result.

[30] For the tropical scenario in DJF (Figure 6e), significant cooling occurs across the entire tropics in the year after the event (season 1). Across the NH middle and high latitudes, the temperature anomaly pattern is zonally asymmetric. Significant cooling occurs over Alaska and Canada, south of Greenland and the Middle East. Little change or slight warming occurs over western Europe, Scandanavia and eastern Siberia. As mentioned above, the winter warming pattern is commonly considered to be a robust response to tropical volcanic eruptions [e.g., *Robock*, 2000; *Stenchikov et al.*, 2002]. This pattern resembles the temperature anomalies associated with the positive phase of the Northern Annular Mode (NAM), which implies a strengthening of the NH polar vortex. Tropical eruptions may excite the positive phase of the NAM in winter by increasing the equator-pole temperature gradient in the lower stratosphere [e.g., *Robock*, 2000]. However, this mechanism may not explain the dominant patterns in our results, as our events may be large enough that radiative effects dominate over dynamical impacts. In particular, the 1258 perturbation is large and lasts for several years (Figure 3e), suggesting that the ocean and sea ice have time to adjust to the reduced shortwave radiation. Interestingly, the DJF SAT anomaly patterns in the high-latitude NH for season 1 of the high-latitude scenario (Figure 6g) and season 2 of the tropical scenario (Figure 6f) are similar, but opposite in sign, to anomalies in a CCSM3 simulation forced by decreased sea-ice albedo (causing decreases in ice extent [*Bitz et al.*, 2006]). Below in section 3.5, we will discuss the role of sea ice in explaining the temperature patterns.

3.2. Zonal-mean Temperature and Zonal Wind

[31] To further explore the possible mechanisms of the surface temperature response, we next consider the vertical profiles of temperature and zonal wind. The characteristic signature of volcanic eruptions in atmospheric temperature is stratospheric warming and tropospheric cooling [*Robock*, 2000; *Santer et al.*, 2003]. Figure 7 shows zonal mean vertical profiles of temperature anomalies for DJF and JJA for both scenarios, composited for the four volcanic episodes. For the tropical scenario in JJA (Figure 7a), there is large stratospheric warming centered at the equator and tropospheric cooling of up to 2.5°C in the tropics. By season 2 (Figure 7b), the stratospheric warming increases in the high latitudes and the tropospheric cooling becomes significant across nearly all latitudes. The magnitude of the cooling is greatest near 300–400 hPA in the tropics and near the surface at the north pole. The high-latitude scenario is associated with significant stratospheric warming centered at 60°N and 60°S (Figure 7c), while tropospheric cooling is significant only poleward of 20°N. By season 2 (Figure 7d), the high-latitude scenario shows a generally weaker version of season 1.

[32] For the tropical scenario in DJF (Figure 7e), there is widespread significant tropospheric cooling. The polar stratosphere and upper troposphere show significant cooling, a pattern that resembles the anomalies associated with

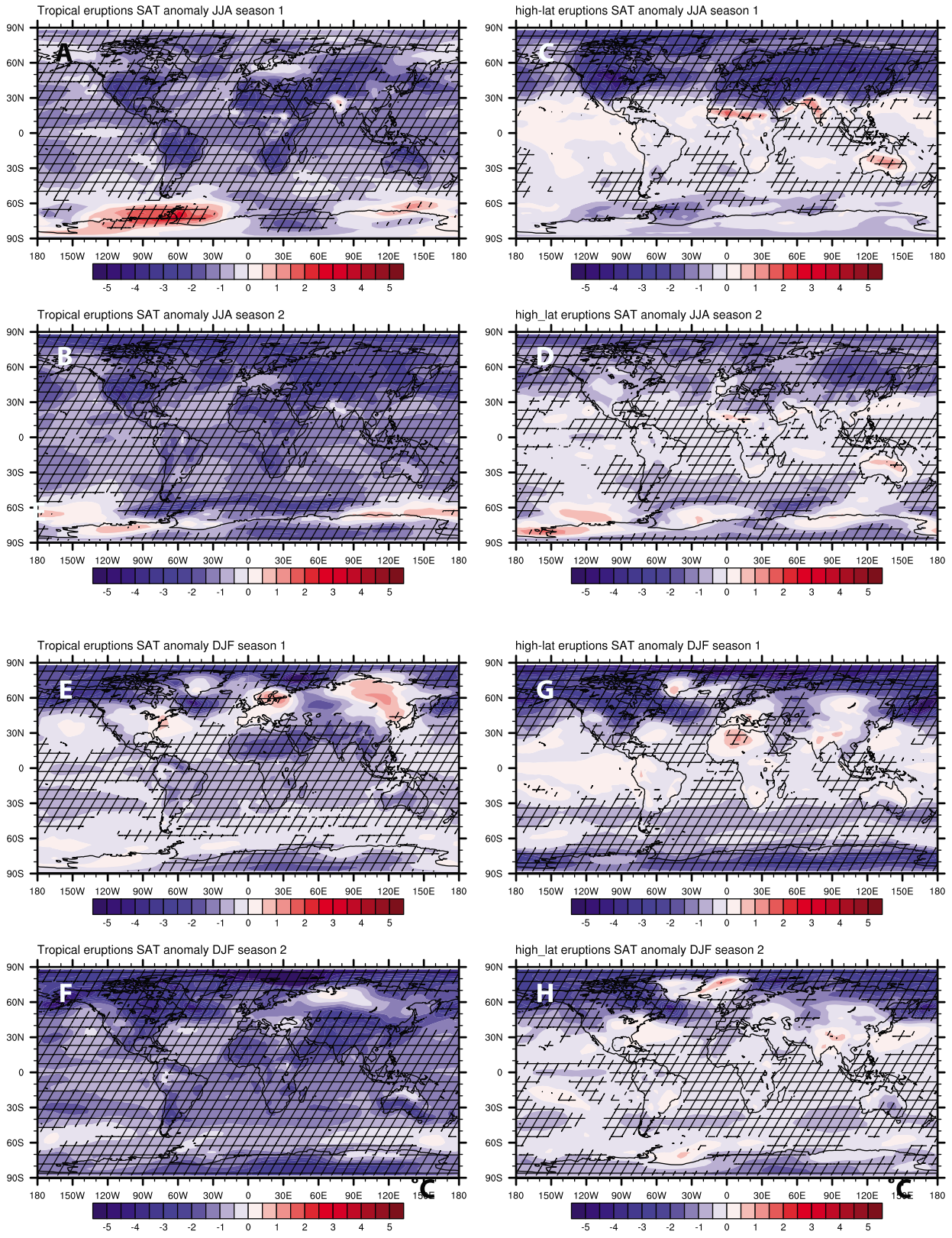

Figure 6. Composites of near-surface temperature anomalies for one and two winter and summer seasons after all eruptions in (left) the tropical scenario and (right) the high-latitude scenario. Tropical scenario JJA (a) season 1 and (b) season 2. High-latitude scenario JJA (c) season 1 and (d) season 2. Tropical scenario JJA (e) season 1 and (f) season 2. High-latitude scenario JJA (g) season 1 and (h) season 2. The color scale is in °C. Anomalies that pass a local Student's *t*-test at the 95% level or above are marked with cross-hatching, assuming that each eruption and each model realization are independent samples.

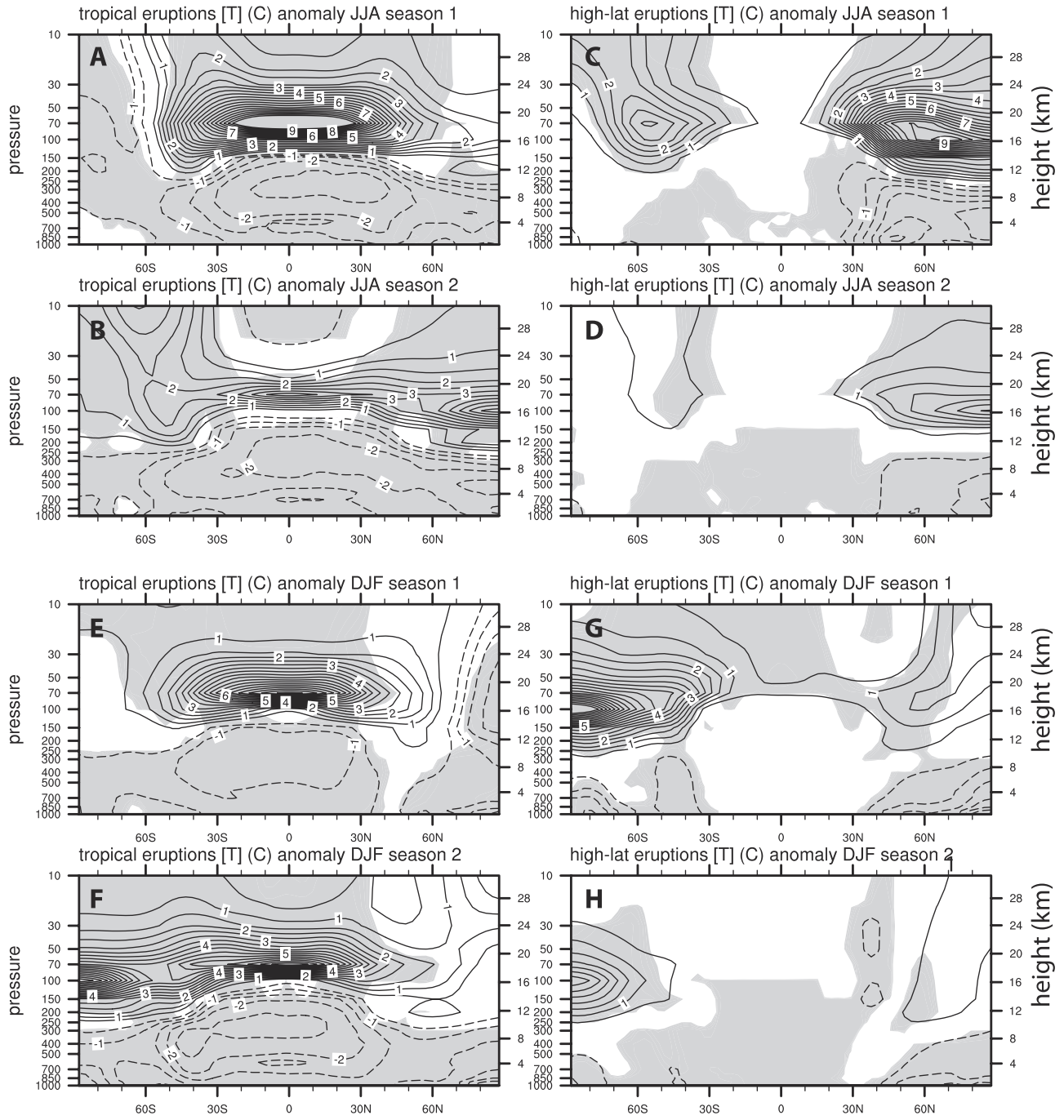

Figure 7. As in Figure 6, but for zonal mean temperature versus height. Anomalies that pass a local Student's *t* test at the 95% level or above are shaded.

the positive phase of the annular mode [e.g., *Thompson and Wallace*, 2000]. However, the composite also shows significant cooling near the surface poleward of 70°N, an effect probably associated with sea ice. By season 2 (Figure 7f), the polar stratospheric cooling disappears as stratospheric warming occurs across all latitudes. Tropospheric cooling is significant at nearly all latitudes. In the NH, the magnitude of cooling increases toward the surface and toward the north pole, an effect not mirrored in the SH winter (Figure 7b). For the high-latitude scenario in DJF (Figure 7g), the largest and most significant cooling occurs near the surface poleward of 50°N.

[33] The DJF anomalies persist longer than the JJA anomalies; in season 2 (Figure 7h) there is significant near-surface cooling in the NH polar region and in the SH midlatitudes. In the extratropics, it is apparent that the near-surface anomalies of the tropical eruptions in season 2 (Figure 7f) resemble the anomalies of the high-latitude eruptions in season 1 (Figure 7g), a feature that is also noticeable on the surface temperature maps (Figure 6), probably due to the long duration of the aerosol transport in the tropical scenario, and thus the lagged response of the extratropics to the forcing. Thus, in our tropical eruption scenario, the stratospheric temperature gradient is short-

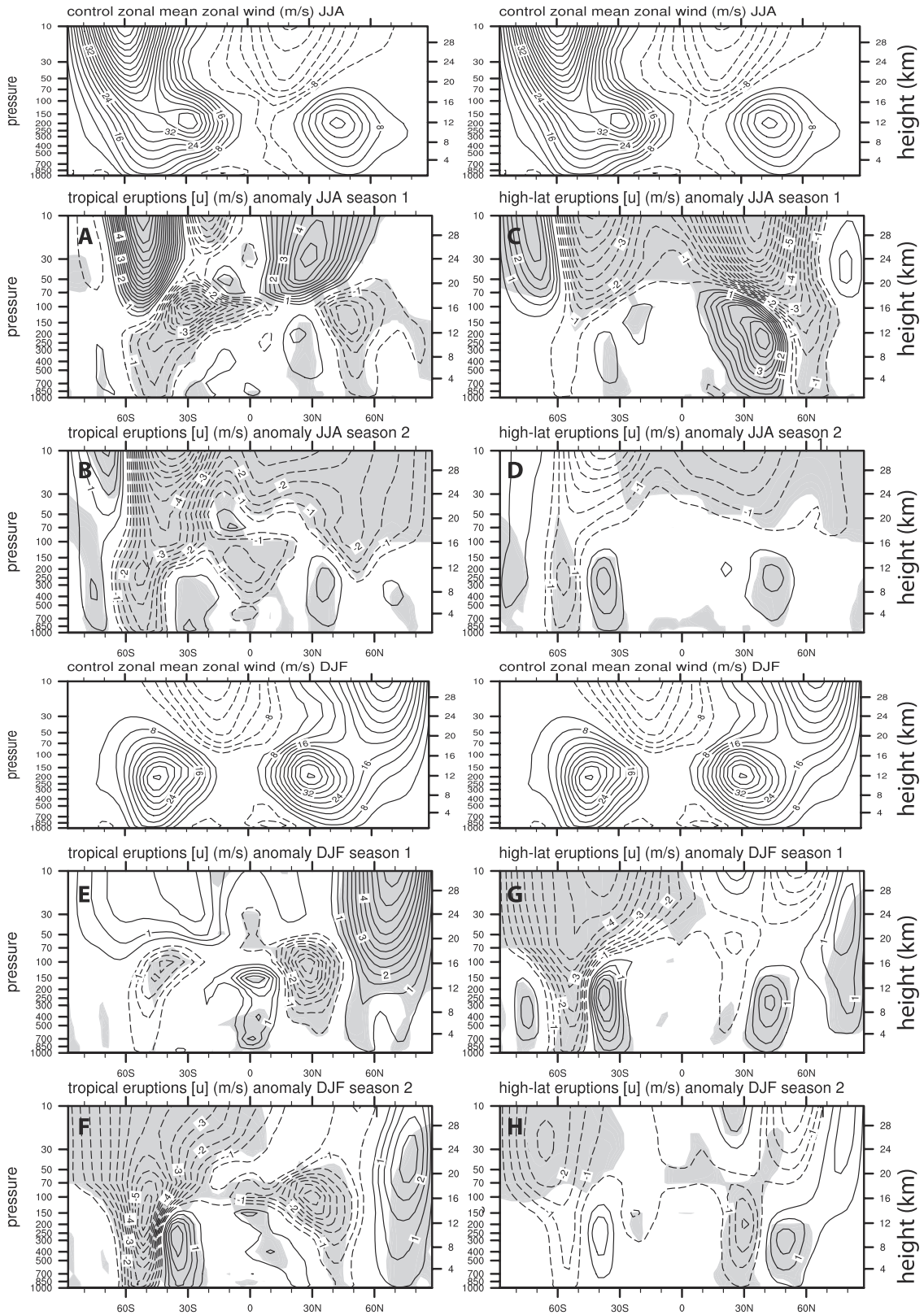

Figure 8. As in Figure 7, but for zonal mean zonal wind versus height. For reference, also shown are the model's climatological zonal winds from the control run.

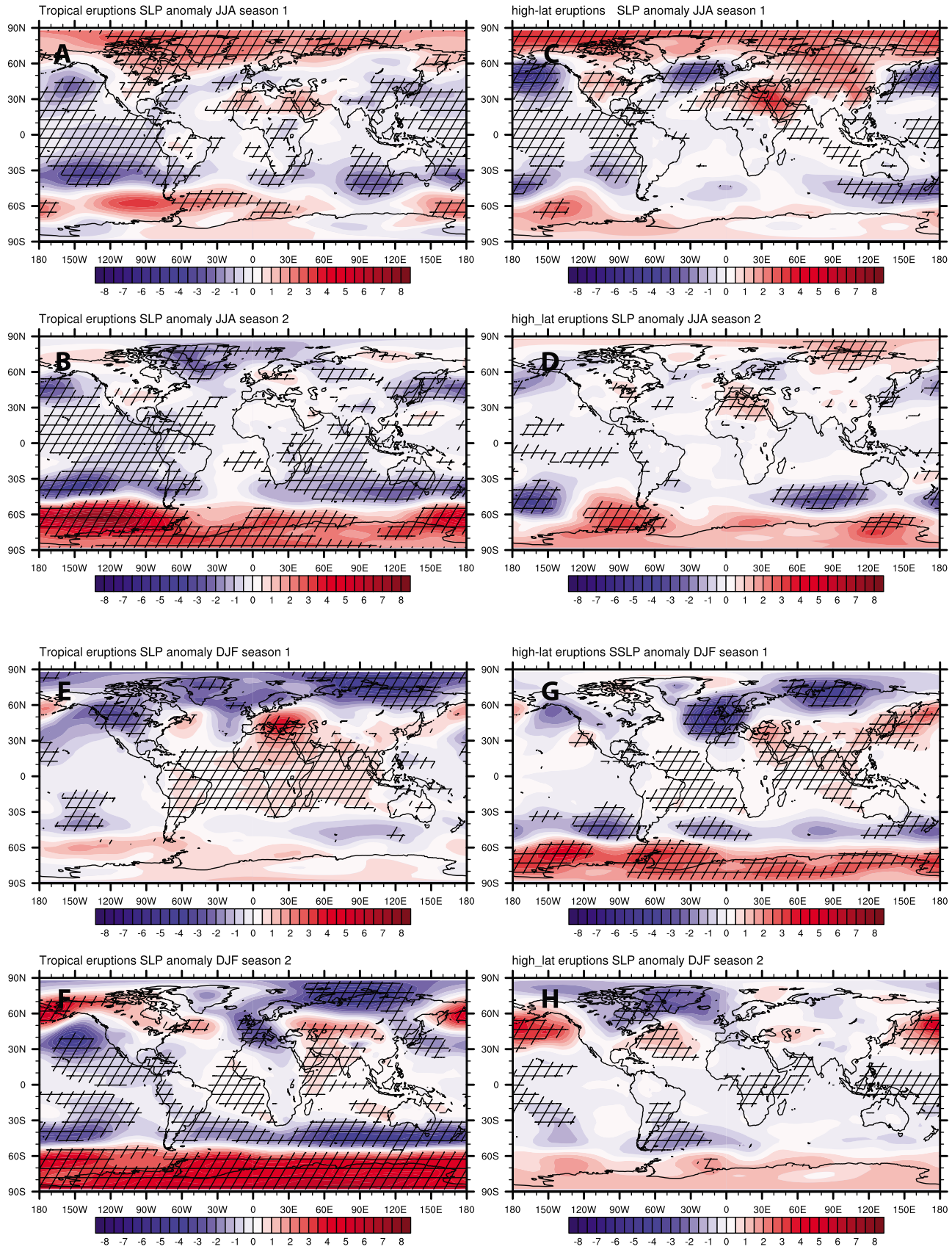

Figure 9. As in Figure 6, but for sea level pressure in hPA.

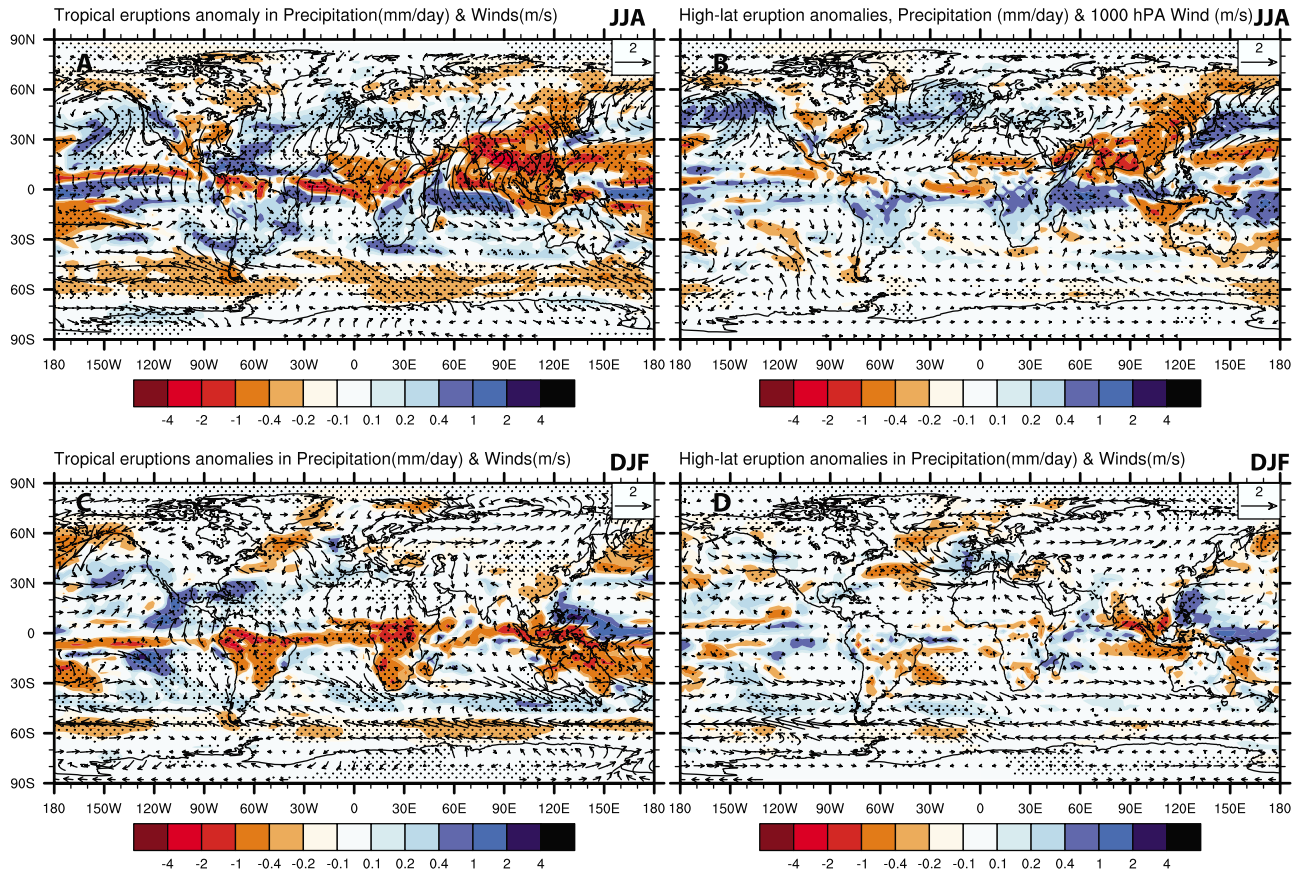

Figure 10. Composites of precipitation (color scale, mm/day) and 1000-hPA-level wind anomalies (arrows, m/s) following (left) tropical eruptions and (right) high-latitude eruptions averaged for two JJA and DJF seasons. (a) Tropical eruptions JJA, (b) high-latitude eruptions JJA, (c) tropical eruptions DJF, (d) high-latitude eruptions DJF. Areas with significant precipitation anomalies passing a local Student's *t* test at the 95% level or above are marked with stippling.

lived, suggesting that the surface climate is not perturbed in the long term via changes to the NAM.

[34] Anomalies in zonal mean zonal wind after volcanic eruptions have been largely attributed to anomalous stratospheric heating [*Haigh et al.*, 2005] and enhanced equator-pole temperature gradients [*Robock*, 2000]. Figure 8 shows zonal mean vertical profiles of zonal wind anomalies for DJF and JJA for both scenarios. For the tropical scenario in JJA (Figure 8a), zonal winds strengthen in the upper stratosphere of the subtropics in season 1, but weaken by the next year after the eruption (Figure 8b). The midlatitude winds are weaker from the tropopause region downward to the surface. For the high-latitude scenario in JJA (Figure 8c), zonal mean zonal winds decrease in the stratosphere from 60°N to 60°S, and slightly increase poleward of 70°N and 70°S. In the troposphere, the winds strengthen equatorward of the subtropical jet core and weaken poleward of the jet core.

[35] For the tropical scenario in DJF (Figure 8e), zonal mean zonal winds increase significantly in the region of the NH polar stratospheric jet and weaken in the region of the subtropical jets of both hemispheres. The pattern of increasing anomalies with height in the NH polar region resembles the signature of the annular mode. Anomalous westerly circulation is present in the equatorial troposphere. By season 2 (Figure 8f), the westerly circulation anomalies in the NH high latitudes weaken, but tighten somewhat, being confined to poleward of 60°N. This general decrease of circulation anomalies in the NH high latitudes from season 1 to season 2 after the eruptions stands in contrast to the increasing strength of the troposphere temperature anomalies, suggesting that the circulation anomalies are not the only driving mechanism of the lower troposphere temperature anomalies. In the high latitudes of the SH the stratospheric circulation weakens significantly, consistent with the delayed arrival of the volcanic aerosols over the summer polar region.

[36] The high-latitude scenario produces less significant change in the zonal mean zonal winds in DJF (Figures 8g–8h). As for the temperature response, the overall pattern of zonal mean zonal wind anomalies of the high-latitude scenario in season 1 resembles that of the tropical scenario in season 2. One apparent difference is that the high-latitude scenario shows a slight increase in the tropospheric westerlies centered at ~40°N that is not present in the tropical scenario, probably due to the edge of the aerosol cloud and temperature gradient present at this latitude for high-latitude eruptions.

3.3. Sea Level Pressure

[37] The changes in SLP are shown in Figure 9. For the tropical scenario in JJA (Figure 9a), there are increases in SLP over the Arctic, northern Africa and the Middle East,

Table 4. Change in Precipitation on Land (mm/day and Percent) for Tropical Eruptions

	JJA	DJF	ANN
NH tropics land (0°–20°N)	−0.72 (−16%)	−0.30 (−23%)	−0.49 (−16%)
SH tropics land (0°–20°S)	−0.33 (−21%)	−1.07 (−15%)	−0.64 (−14%)
Global land	−0.22 (−11%)	−0.23 (−11%)	−0.21 (−10%)
NH extratropics land (20°–60°N)	−0.15 (−7%)	−0.19 (−2%)	−0.07 (−4%)
SH extratropics land (20°–60°S)	−0.01 (−1%)	−0.43 (−13%)	−0.13 (−7%)

and in a belt at ∼60°S. Decreases occur over the ocean basins, consistent with the temperature changes. By season 2 (Figure 9b), the Arctic SLP anomalies switch sign, while the SH SLP anomalies strengthen. The high-latitude scenario produces similar anomalies, except that they are stronger in the NH (Figures 9c–9d). Anomalous high pressure occurs over the eastern Mediterranean, Middle East, Asia, and North America. This may be understood as a consequence of reduced summer heating over the continent with the reduction in shortwave radiation reaching the surface, leading to less rising motion. This pattern has implications for the summer precipitation anomalies, as discussed below.

[38] The tropical scenario in DJF (Figure 9e) produces significant reductions in pressure over the North Atlantic, Greenland, the North Pacific, North America and in the zone from 30° to 40°S. Significant increases occur over the Middle East, Africa, Indian Ocean and the Antarctic continent. The pattern resembles the NAM in that there are pressure reductions across the Arctic. However, the strong pressure contrast in the North Atlantic associated with the NAM is not evident. Instead, a pressure contrast occurs across central Europe, with associated anomalous southerly winds and weak warming (Figure 6). The high-latitude scenario (Figures 9g–9h) produces similar patterns over the Southern Ocean, the Middle East and the Western Europe/North Atlantic region that become much weaker by season 2.

3.4. Precipitation and Winds

[39] The volcanic aerosol forcing produces large changes in precipitation patterns across the globe, with some similar patterns for the tropical and high-latitude scenario if the two years after the eruptions are averaged (Figure 10). There are large reductions in precipitation over the summer monsoon regions and over the SH storm track, which shifts equatorward in both seasons. Reductions also occur across the NH high-latitude landmasses in summer (JJA, Figures 10a, 10b) and at the end of the northeast Atlantic storm track in the NH winter (DJF, Figures 10c, 10d). Overall, global precipitation is reduced; however, there are increases in the subtropics in the SH winter (JJA; Figures 10a, 10b) just north of the equator in the NH winter (DJF; Figures 10c, 10d) and over the NH midlatitude oceans in summer (JJA, Figures 10a, 10b). By comparing Figure 10 to the vertical profile of zonal wind in Figure 8, it is apparent that the zones of stronger westerly flow correspond to areas of increased precipitation and vice versa. This is especially pronounced in the SH summer (DJF; compare Figures 8 (e–h) to Figures 10c, 10d): in the zone 50°–60°S precipitation is reduced and the flow throughout the lower troposphere is anomalously easterly; in the zone 30°–40°S, precipitation is slightly increased and the tropospheric flow is anomalously westerly; from near the equator to 10°N, precipitation is increased and the flow is anomalously westerly. The NH summer exhibits a weaker version of this pattern with some notable zonal asymmetry. Comparing the NH in Figure 8c to the SH in Figure 8e or Figure 8g, the similar behavior of the zonal shift of the winds in the respective summer seasons is apparent. Given its limited seasonal cycle, the SH winter response is similar to the SH summer response, while in the NH winter, there is a NAM-like response in the zonal wind.

[40] Given the large forcing, the reduction in precipitation over land is significant, and we quantify the amount in Tables 4 and 5 for both the tropical and high-latitude scenarios. The first-order difference is that the tropical scenario produces much larger reductions over most latitudes. The exception is the NH extratropics in summer; the high-latitude scenario response is on par with the tropical scenario response, consistent with the strong local forcing over the NH of the high-latitude eruptions, the large changes in surface temperature and changes in SLP. Across the summer monsoon region over tropical land, the reduction in zonal mean precipitation is on the order of 15%, and certainly larger than this over southeast Asia. In the low-level wind field, the flow is anomalously from land to sea. The larger absolute reductions in precipitation over tropical land are in the summer, but percentage-wise the reductions are greater in the winter.

[41] As the largest absolute reductions in precipitation occur in the summer, it is clear that the response is driven directly by the reduction in shortwave radiation caused by the aerosols. The anomalously dry zone is not just on land, but extends across the ocean basins, from about the equator to 20°S in DJF, and the equator to 10°N in JJA. This suggests that the normal seasonal migration of the Intertropical Convergence Zone (ITCZ) into the summer hemisphere is restricted, because there is relatively more cooling in the low-mid latitudes of the summer hemisphere than in the winter hemisphere. The precipitation anomaly pattern is

Table 5. Change in Precipitation on Land (mm/day and Percent) for High-Latitude Eruptions

	JJA	DJF	ANN
NH tropics land (0°–20°N)	−0.12 (−2.7%)	−0.09 (−7%)	−0.06 (−2%)
SH tropics land (0°–20°S)	−0.02 (−1%)	−0.07 (−1%)	−0.01 (0.2%)
Global land	−0.12 (−6%)	−0.05 (−2%)	−0.05 (−2.5%)
NH extratropics land (20°–60°N)	−0.17 (−8%)	−0.01 (−1%)	−0.05 (−3%)
SH extratropics land (20°–60°S)	−0.08 (−7%)	−0.13 (−4%)	−0.06 (−3%)

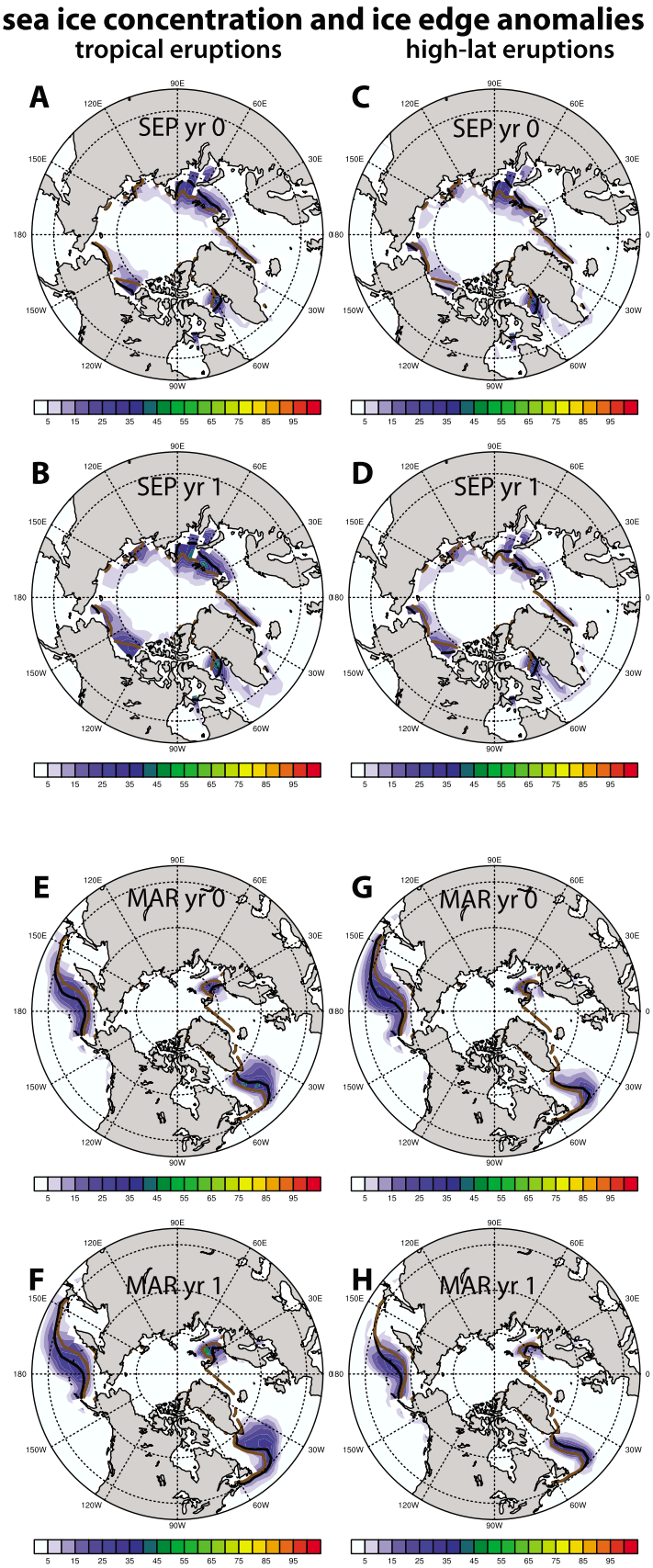
sea ice concentration and ice edge anomalies
tropical eruptions
high-lat eruptions
A
SEP yr 0
C
SEP yr 0
B
SEP yr 1
D
SEP yr 1
E
MAR yr 0
G
MAR yr 0
F
MAR yr 1
H
MAR yr 1
90E
120E
60E
150E
30E
180
0
150W
30W
120W
60W
90W
5 15 25 35 45 55 65 75 85 95

Figure 11

associated with a combination of global cooling and thus decreased evaporation, reduction in the strength of the monsoon circulations, restricted seasonal migration of the ITCZ into the summer hemisphere, and a contracted Hadley Cell.

3.5. Sea Ice

[42] As suggested above, sea ice appears to play a strong modifying role in the climatic response to volcanic aerosol forcing. Figure 11 shows the pattern of changes in NH sea ice concentration and the expansion of the ice edge for the minimum (September) and maximum (March) ice months for both the tropical and high-latitude scenarios. Figure 12 shows the time series of ice extent for March and September for each scenario. It is apparent that the tropical eruptions produce a larger and more persistent response, especially in March. By the end of the 50-year simulation (14 years after the last eruption), the tropical scenario still has 10^6 km^2 more ice cover in March than the average of the control simulation (Figure 12b); in September the difference is about a half a million km^2 (Figure 12a). The simulations have not been run out longer, but this suggests that even in the absence of further changes in forcing, a significant change in ice cover would persist for at least another decade or longer, cooling the climate. The ice area for the high-latitude eruptions is significantly larger than the control simulation only for up to a decade after eruptions, so this scenario would unlikely have a long-term climatic impact.

[43] The spatial patterns of ice concentration response for the tropical and high-latitude scenarios are similar (Figure 11). As for many of the other variables, the anomalies associated with the tropical eruption build from season 1 to season 2 and the anomalies associated with the high-latitude eruptions decrease. The summer pattern of ice concentration anomalies (Figures 11a–11d) increases around the margins of the Arctic basin. This is associated with cooling in the High Arctic (80°–90°N) that is evident in the surface temperature pattern (Figures 6b–6c). In winter, the ice concentration increases in the marginal seas, south of Greenland and in the Aleutian island chain and Sea of Japan (Figures 11e–11h). These regions of increased ice closely match the areas of strong cooling in the NH, contributing to the zonally asymmetric appearance of the temperature anomalies (Figures 6e–6h). The reduction in the strength, and even change of sign, of SLP and 500-hPA geopotential height anomalies (Figures 9e–9h and Figures 8a–8b) from season 1 to season 2 suggests that the ice concentration change is more of a thermodynamic than a dynamic response. In experiments where ice concentration is deliberately changed (by changing the albedo parameters, which is qualitatively similar to changing the SW forcing), sea ice and surface temperature show a qualitatively similar pattern as the results here [*Bitz et al.*, 2006]. However, our results, especially for the tropical scenario, also show a more global pattern of temperature anomalies than is produced just by reducing sea-ice albedo. The global pattern is qualitatively similar to the pattern produced by the double CO_2 experiment of *Bitz et al.* [2006], albeit in the other direction.

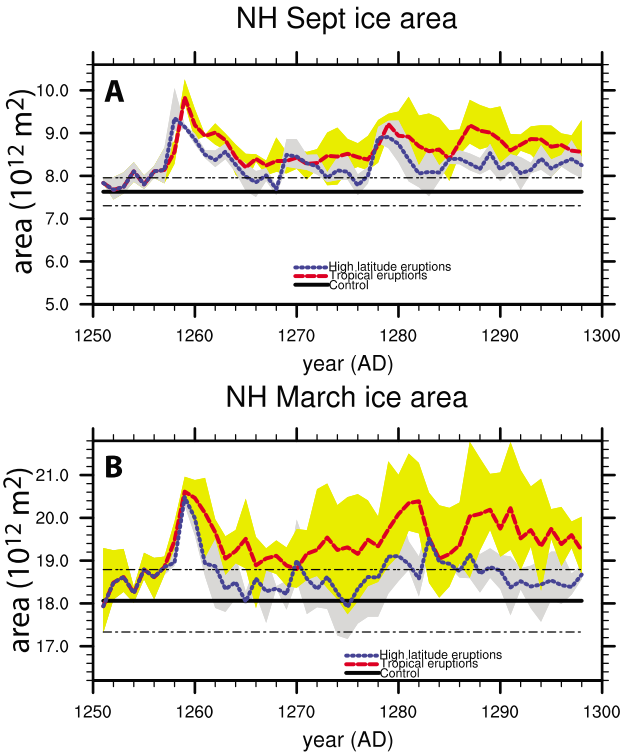

Figure 12. Time series of the area of NH sea ice (area with >15% ice concentration) for (a) September and (b) March for the ensemble mean of the tropical scenario (red lines) and the ensemble mean of the high-latitude scenario (blue lines). The yellow shading for tropical scenario and gray shading for the high-latitude scenario represents the spread of the individual ensemble members. The solid black line represents the mean of the control simulation, and the dashed black lines indicate ±1 standard deviation of the control simulation's NH ice area.

4. Summary and Discussion

[44] We have used a fully coupled climate model, the NCAR Community Climate System Model, Version 3, to investigate the climatic response to large volcanic eruptions in the preindustrial background climate state. This study builds upon previous model-based studies of volcanic eruptions and climate by focusing on the second half of the 13th century, which was likely the most volcanically perturbed half-century of the last 1000 years, by performing a systematic comparison of the radiative and dynamical effects of

Figure 11. Composites of sea ice concentration (%, color scale) and sea ice edge anomalies (location of the 50% ice concentration contour, brown lines) for the maximum (March) and minimum (September) months following (left) tropical and (right) high-latitude eruptions. Also shown is the location of the 50% ice concentration contour in the control simulation (black lines). Tropical eruptions SEP (a) season 1 and (b) season 2. High-latitude eruptions SEP (c) season 1 and (d) season 2. Tropical eruptions MAR (e) season 1 and (f) season 2. High-latitude eruptions MAR (g) season 1 and (h) season 2.

eruptions at high latitudes and low latitudes, and by using a fully coupled model at relatively high horizontal resolution rather than a stand-alone atmospheric model.

[45] Our simulations facilitate the direct comparison of the impacts of tropical and high-latitude eruptions and the consideration of the long-term effects of closely sequenced eruptions. To summarize the results:

[46] 1. In either scenario (tropical or high-latitude events) the Arctic is the most impacted latitude band in the winter, because of the ice-albedo feedback and changes in the circulation of the atmosphere and the ocean.

[47] 2. In both scenarios, there is significant cooling over the continents in summer.

[48] 3. The impacts of large high-latitude eruptions are largely restricted to the short-term, even in the Arctic, whereas large and closely spaced tropical eruptions could have long-term impacts.

[49] 4. The high-latitude scenario produces very little significant change in the climate of the Southern Hemisphere, except over the Southern Ocean where the westerlies shift equatorward. There is also a small cooling signal over New Zealand and southern Australia.

[50] 5. In the winter, the relative impacts of direct radiative forcing and dynamical changes are different for very large tropical eruptions compared with smaller eruptions. The winter warming pattern associated with the stronger polar vortex occurs 1–2 seasons after the smaller events, but it does not appear after the very large (1258 AD) event.

[51] 6. The dynamical impacts of tropical eruptions, such as the positive phase NAM and the winter warming pattern, are short-lived, and all tropical eruptions produce global-average cooling. We suggest that the relative dominance of thermodynamics is enhanced by the preindustrial climate state, which has more sea ice and snow than the modern, and no ozone depletion to enhance the stratospheric equator-pole temperature gradient.

[52] 7. In addition to causing global cooling, large tropical events significantly alter the hydrological cycle, associated with reduced precipitation over land, especially in the tropics. Large high-latitude events have a similar, but much less severe, pattern of impacts on tropical precipitation.

[53] The major differences in the timing and magnitude of the response are linked to the prescribed transport of the lower stratospheric aerosols; in the tropical scenario they originate at low latitudes and migrate poleward, while in the high-latitude scenario, the aerosols are confined to the extratropics of each hemisphere and they do not last very long. Either scenario is consistent with the available ice core records. The impacts of high-latitude volcanism fade relatively quickly, whereas the impacts of tropical volcanism build from the first year after the eruption to the second year after the eruption. The spatial patterns of the response to the tropical eruptions in the second year mimic the patterns of the first year after the high-latitude event. In our simulations, this lagged and strengthened extratropical response to tropical eruptions is further exaggerated by the growth of NH sea ice and the lowering of SSTs. The expanded NH sea ice is associated with a strong equator-pole temperature gradient near the surface, such that the Arctic cools much more than the tropics, especially in the NH winter. In the tropical scenario, significant cooling of the Arctic and expanded NH sea ice persists until the end of the simulation, more than a decade after the last volcanic pulse, suggesting that volcanism is a plausible driver of long-term climate change in the Arctic. Conformation of this result will require longer integrations and a more detailed examination of some of the feedback mechanisms involved, such as changes in the ocean heat transport to the Arctic, which in present-day simulations is very important for maintaining the ice cover [e.g., *Holland et al.*, 2006b].

[54] These results show significant dynamical responses associated with tropical volcanic eruptions, particularly in regards to the NAM, in agreement with previous studies [e.g., *Robock*, 2000; *Stenchikov et al.*, 2002, 2006; *Shindell et al.*, 2003]. Changes in sea level pressure, zonal mean temperature, zonal mean zonal winds, geopotential height, and near-surface air temperature are all consistent with the positive phase of the NAM (Table 3). The response to the smaller events is in general agreement with the observations presented by *Stenchikov et al.* [2006], although it is not possible to make an exact comparison because of the different climate states and different eruption magnitudes between the 20th century and the simulated 13th century, and because of sampling issues in the observations. The large 1258 event produces a negative anomaly in polar SLP and geopotential height in the first winter season, but it is weaker than for the smaller events, and the winter warming pattern is absent. This suggests that even in the winter the direct radiative effects dominate the net surface temperature response for very large tropical eruptions, in general agreement with *Shindell et al.* [2003]. We also find a significant increase in the NH sea-ice area, a result not reported in previous work.

[55] Recent studies have paid increased attention to the response of the hydrological cycle to volcanic eruptions [e.g., *Oman et al.*, 2005, 2006b; *Trenberth and Dai*, 2007] or to idealized sulfate aerosol geoengineering schemes [e.g., *Bala et al.*, 2008; *Robock et al.*, 2008]. *Oman et al.* [2005, 2006a, 2006b] report significant reductions in precipitation in the African and Asian monsoon regions in response to the high-latitude Katmai, Alaska eruptions of 1912 and the Laki, Iceland eruption of 1783. A similar signal is also found in response to the injection of sulfate aerosols into the Arctic stratosphere [*Robock et al.*, 2008]. In the high-latitude eruption scenario, we also find significantly reduced precipitation in the NH summer monsoon regions as well as across eastern Asia and other NH continental regions. There is a much weaker signal in the SH summer (DJF).

[56] In the tropical scenario, we find reductions in precipitation over land of more than 20% in the zonal mean and greater than this in some regions, including India and SE Asia. The spatial pattern of precipitation anomalies agrees well with that reported in observations of the response to the Pinatubo eruption [*Trenberth and Dai*, 2007], and results from other models [*Robock et al.*, 2008]. Overall, our results are consistent with the known climatic impacts of major volcanic eruptions.

[57] In the context of the 13th century, our results point to some additional ways that proxy records could be used to clarify the role of volcanism in the climate transition from the relatively warm Medieval times to the colder Little Ice Age. The apparently massive 1257/58 event has not been attributed to a specific source volcano, making it difficult to believe the sulfate as the primary evidence for a huge tropical

eruption. To help identify the source(s) it will be necessary to use additional methods, such as geochemical fingerprinting of tephra. Besides identifying the volcano(es), it is important to synthesize the available proxy records to determine the magnitude and spatial patterns of change. Our results present one framework against which the proxy network could be compared to assess the underlying physical mechanisms of change, showing the patterns of change due to volcanism alone. While a synthesis of proxy data is beyond the scope of this paper, existing records do hold some clues.

[58] In terms of the climate response to the 1257/58 event, it is first notable that *Stothers* [2000] presents documentary evidence for severe winter cooling in Europe, crop failures, disease, and other social problems apparently following the 1258 eruption. Severe winters in Europe are more consistent with the response to an exceptional, very large tropical event like we simulated for 1258 than with the winter warming pattern that tends to occur for two winters after the more common smaller magnitude eruptions. High-latitude eruptions, even if very large, do not seem to produce strong cooling over Europe except during the first summer (Figure 6). Second, a huge tropical eruption would likely cause a major perturbation to the global hydrological cycle, significantly reducing precipitation in the tropics and causing a general drying over most land areas. Such a signal should be identifiable in proxy and documentary records. As an example, *Oman et al.* [2006a] present evidence for lower water flows in the Nile River following the Laki, Iceland eruption of 1783.

[59] Third, the spatial pattern of the temperature change is an important indicator of the type of forcing. As previously discussed, the expected major cooling from the 1257/58 event is not readily apparent in reconstructions of NH temperatures. However, new data from the Arctic do indicate cooling at that time, suggesting there were at least regional changes, possibly consistent with the greater temperature changes in the Arctic than at lower latitudes in our volcanic scenarios. The data assimilation and model results of *Crespin et al.* [2009] indicate Arctic cooling of about 0.5° C from about 1250 to 1300 AD, followed by a warming in the 14th and 15th centuries. New records from lake sediment [e.g., *Kaufman*, 2009] can be also be used to assess temperature changes in the Arctic. *Anderson et al.* [2008] found evidence for significant ice cap expansion on Baffin Island commencing before 1300 AD. In our model simulations, the North Atlantic and Canadian Archipelago region experiences strong winter as well as summer cooling, amplified by the regional sea-ice response. Such strong and persistent cooling in both winter and summer is not as evident in the Alaskan region, where the Aleutian Low plays the dominant role in the regional climate variations. In southern Alaska in particular, the climate is relatively maritime and is strongly influenced by the Pacific, while the Canadian Archipelago is surrounded by thick sea ice and has a more continental climate regime, situated on the polar side of the North Atlantic storm track. Thus one would expect to find different proxy signatures (or possibly none) of volcanic forcing in the Alaskan region because the response to the forcing is moderated by the proximity to the open ocean. Additionally, the response of the sea ice is key to understanding the Arctic climate response to volcanic forcing. There are some indicators of severe ice years in Iceland in the latter half of the 13th century [*Ogilvie and Jonsson*, 2001]. Although our simulations do not indicate increased sea-ice concentration around Iceland (Figure 11), this is qualitatively consistent with the climate cooling. *Masse et al.* [2008] and *Jiang et al.* [2005] present proxies of SST and sea ice near Iceland, showing increases in sea-ice concentration and decreases in SST near the end of the 13th century, the time that *Masse et al.* [2008] interpret as a transition from the warm period to the Little Ice Age, in accordance with other authors [e.g., *Grove*, 2001].

[60] Ongoing work includes simulations that include solar and orbital forcing, and investigations that focus on the response of the extratropical NH atmospheric circulation. Expected improvements to the CCSM include the implementation of particle size evolution, which will enable experiments that explicitly test the assumptions about the forcing for very large volcanic events such as the 1258 AD event. In part to address possible shortcomings in the atmospheric model's dynamical simulations, we also plan simulations with the Whole Atmosphere Community Model, which has a well-resolved stratosphere and options for interactive chemistry and aerosols [e.g., *Richter et al.*, 2008]. As more proxy data are collected, linking the climatic response in the simulations with the climatically sensitive processes that are actually recorded by the proxies will be a major challenge to overcome in arriving at a complete, physically consistent explanation of climate change over the past millennium.

[61] **Acknowledgments.** Funding for this project was provided by the National Science Foundation, Office of Polar Programs, through grants ARC-0455043 (supporting D.S.K.) and ARC-0454930 (supporting B.L.O., C.M.A. and D.P.S.). Computing time and facilities were provided by NCAR's Computational and Information Systems Laboratory through project number 37001001 and by the CCSM's Paleoclimate Working Group. The National Center for Atmospheric Research is sponsored by the National Science Foundation. We thank Jian Lu for providing a thoughtful review of a draft of this paper, and three anonymous reviewers for their constructive suggestions that led to an improved manuscript.

References

Alexander, M., J. Yin, G. Branstator, A. Capotondi, C. Cassou, R. Cullather, Y. O. Kwon, J. Norris, J. Scott, and I. Wainer (2006), Extratropical atmosphere-ocean variability in CCSM3, *J. Clim.*, *19*(11), 2496–2525.

Ammann, C. M., G. A. Meehl, W. M. Washington, and C. S. Zender (2003), A monthly and latitudinally varying volcanic forcing dataset in simulations of 20th century climate, *Geophys. Res. Lett.*, *30*(12), 1657, doi:10.1029/2003GL016875.

Ammann, C. M., F. Joos, D. S. Schimel, B. L. Otto-Bliesner, and R. A. Tomas (2007), Solar influence on climate during the past millennium: Results from transient simulations with the NCAR Climate System Model, *Proc. Natl. Acad. Sci. U. S. A.*, *104*(10), 3713–3718.

Anderson, R. K., G. H. Miller, J. P. Briner, N. A. Lifton, and S. B. DeVogel (2008), A millennial perspective on Arctic warming from ^{14}C in quartz and plants emerging from beneath ice caps, *Geophys. Res. Lett.*, *35*(1), L01502, doi:10.1029/2007GL032057.

Arblaster, J. M., and G. A. Meehl (2006), Contributions of external forcings to southern annular mode trends, *J. Clim.*, *19*(12), 2896–2905.

Bala, G., P. B. Duffy, and K. E. Taylor (2008), Impact of geoengineering schemes on the global hydrological cycle, *Proc. Natl. Acad. Sci. U. S. A.*, *105*(22), 7664–7669.

Bitz, C. M., P. R. Gent, R. A. Woodgate, M. M. Holland, and R. Lindsay (2006), The influence of sea ice on ocean heat uptake in response to increasing CO_2, *J. Clim.*, *19*(11), 2437–2450.

Collins, W. D., et al. (2006), The Community Climate System Model version 3 (CCSM3), *J. Clim.*, *19*(11), 2122–2143.

Crespin, E., H. Goosse, T. Fichefet, and M. E. Mann (2009), Potential causes of 15th century Arctic warming using coupled model simulations with data assimilation, *Clim. Past Discuss.*, *5*, 1–27.

Crowley, T. J. (2000), Causes of climate change over the past 1000 years, *Science*, *289*(5477), 270–277.

Crowley, T. J., and K. Y. Kim (1999), Modeling the temperature response to forced climate change over the last six centuries, *Geophys. Res. Lett.*, *26*(13), 1901–1904.

Crutzen, P. J. (2006), Albedo enhancement by stratospheric sulfur injections: A contribution to resolve a policy dilemma?, *Clim. Change*, *77*(3–4), 211–219.

D'Arrigo, R., D. Frank, G. Jacoby, and N. Pederson (2001), Spatial response to major volcanic events in or about AD 536, 934 and 1258: Frost rings and other dendrochronological evidence from Mongolia and northern Siberia: Comment on Stothers, R. B., "Volcanic dry fogs, climate cooling, and plague pandemics in Europe and the Middle East" (Climatic Change, 42, 1999), *Clim. Change*, *49*(1–2), 239–246.

D'Arrigo, R., R. Wilson, and G. Jacoby (2006), On the long-term context for late twentieth century warming, *J. Geophys. Res.*, *111*, D03103, doi:10.1029/2005JD006352.

Deser, C., and A. S. Phillips (2009), Atmospheric Circulation Trends, 1950–2000: The relative roles of sea surface temperature forcing and direct atmospheric radiative forcing, *J. Clim.*, *22*, 396–413.

DeWeaver, E., and C. M. Bitz (2006), Atmospheric circulation and its effect on Arctic sea ice in CCSM3 simulations at medium and high resolution, *J. Clim.*, *19*(11), 2415–2436.

Gao, C., A. Robock, and C. Ammann (2008), Volcanic forcing of climate over the past 1500 years: An improved ice core-based index for climate models, *J. Geophys. Res.*, *113*, D23111, doi:10.1029/2008JD010239.

Graf, H. F., I. Kirchner, A. Robock, and I. Schult (1993), Pinatubo eruption winter climate effects—model versus observations, *Clim. Dyn.*, *9*(2), 81–93.

Grove, J. M. (2001), The initiation of the "Little Ice Age" in regions round the North Atlantic, *Clim. Change*, *48*(1), 53–82.

Hack, J. J., J. M. Caron, S. G. Yeager, K. W. Oleson, M. M. Holland, J. E. Truesdale, and P. J. Rasch (2006), Simulation of the global hydrological cycle in the CCSM Community Atmosphere Model version 3 (CAM3): Mean features, *J. Clim.*, *19*(11), 2199–2221.

Haigh, J. D., M. Blackburn, and R. Day (2005), The response of tropospheric circulation to perturbations in lower-stratospheric temperature, *J. Clim.*, *18*(17), 3672–3685.

Holland, M. M., C. M. Bitz, E. C. Hunke, W. H. Lipscomb, and J. L. Schramm (2006a), Influence of the sea ice thickness distribution on polar climate in CCSM3, *J. Clim.*, *19*(11), 2398–2414.

Holland, M. M., C. M. Bitz, and B. Tremblay (2006b), Future abrupt reductions in the summer Arctic sea ice, *Geophys. Res. Lett.*, *33*, L23503, doi:10.1029/2006GL028024.

Hurrell, J. W., J. J. Hack, A. S. Phillips, J. Caron, and J. Yin (2006), The dynamical simulation of the Community Atmosphere Model version 3 (CAM3), *J. Clim.*, *19*(11), 2162–2183.

Hyde, W. T., and T. J. Crowley (2000), Probability of future climatically significant volcanic eruptions, *J. Clim.*, *13*(9), 1445–1450.

Jansen, E., et al. (2007), *Climate Change 2007: The Physical Science Basis. Contribution of Working Group I to the Fourth Assessment Report of the Intergovernmental Panel on Climate Change*, chap. 6, edited by S. Solomon et al., 479 pp., Cambridge Univ. Press, Cambridge, U. K.

Jiang, H., J. Eiriksson, M. Schulz, K. L. Knudsen, and M. S. Seidenkrantz (2005), Evidence for solar forcing of sea-surface temperature on the North Icelandic Shelf during the late Holocene, *Geology*, *33*(1), 73–76.

Kaufman, D. S. (2009), An overview of late Holocene climate and environmental change inferred from Arctic lake sediment, *J. Paleolimnol.*, *41*(1), 1–6, doi:10.1007/s10933-008-9259-6.

Kaufman, D. S., et al. (2004), Holocene thermal maximum in the western Arctic (0–180° W), *Quat. Sci. Rev.*, *23*, 529–560.

Kirchner, I., G. L. Stenchikov, H. F. Graf, A. Robock, and J. C. Antuña (1999), Climate model simulation of winter warming and summer cooling following the 1991 Mount Pinatubo volcanic eruption, *J. Geophys. Res.*, *104*(D16), 19,039–19,055.

Kurbatov, A. V., G. A. Zielinski, N. W. Dunbar, P. A. Mayewski, E. A. Meyerson, S. B. Sneed, and K. C. Taylor (2006), A 12,000 year record of explosive volcanism in the Siple Dome Ice Core, West Antarctica, *J. Geophys. Res.*, *111*, D12307, doi:10.1029/2005JD006072.

Langway, C. C., K. Osada, H. B. Clausen, C. U. Hammer, and H. Shoji (1995), A 10-century comparison of prominent bipolar volcanic events in ice cores, *J. Geophys. Res.*, *100*(D8), 16,241–16,247.

Lorenz, S. J., C. Timmreck, T. J. Crowley, J. Jungclaus, S. Kinne, U. Schlese, and M. Thomas (2008), Understanding the climate signal of the 1258 eruption, *Geophysical Research Abstracts, 10*, EGU20080A-08240, (Presented at EGU General Assembly 2008).

Masse, G., S. J. Rowland, M. Sicre, J. Jacob, E. Jansen, and S. T. Belt (2008), Abrupt climate changes for Iceland during the last millennium: Evidence from high resolution sea ice reconstructions, *Earth Planet. Sci. Lett.*, *269*(3–4), 564–568, doi:10.1016/j.epsl.2008.03.017.

Meehl, G. A., W. M. Washington, B. D. Santer, W. D. Collins, J. M. Arblaster, A. X. Hu, D. M. Lawrence, H. Y. Teng, L. E. Buja, and W. G. Strand (2006), Climate change projections for the twenty-first century and climate change commitment in the CCSM3, *J. Clim.*, *19*(11), 2597–2616.

Miller, R. L., G. A. Schmidt, and D. T. Shindell (2006), Forced annular variations in the 20th century IPCCAR4 models, *J. Geophys. Res.*, *111*, D18101, doi:10.1029/2005JD006323.

National Research Council (2006), *Surface Temperature Reconstructions for the Last 2000 Years*, 145 pp., National Acad. Press, Washington, D. C.

Ogi, M., and J. M. Wallace (2007), Summer minimum Arctic sea ice extent and the associated summer atmospheric circulation, *Geophys. Res. Lett.*, *34*, L12705, doi:10.1029/2007GL029897.

Ogilvie, A. E. J., and T. Jonsson (2001), "Little Ice Age" research: A perspective from Iceland, *Clim. Change*, *48*(1), 9–52.

Oman, L., A. Robock, G. Stenchikov, G. A. Schmidt, and R. Ruedy (2005), Climatic response to high-latitude volcanic eruptions, *J. Geophys. Res.*, *110*, D13103, doi:10.1029/2004JD005487.

Oman, L., A. Robock, G. L. Stenchikov, and T. Thordarson (2006a), High-latitude eruptions cast shadow over the African monsoon and the flow of the Nile, *Geophys. Res. Lett.*, *33*, L18711, doi:10.1029/2006GL027665.

Oman, L., A. Robock, G. L. Stenchikov, T. Thordarson, D. Koch, D. T. Shindell, and C. C. Gao (2006b), Modeling the distribution of the volcanic aerosol cloud from the 1783–1784 Laki eruption, *J. Geophys. Res.*, *111*, D12209, doi:10.1029/2005JD006899.

Oppenheimer, C. (2003), Ice core and palaeoclimatic evidence for the timing and nature of the great mid-13th century volcanic eruption, *Int. J. Climatol.*, *23*(4), 417–426.

Otto-Bliesner, B. L., R. Tomas, E. C. Brady, C. Ammann, Z. Kothavala, and G. Clauzet (2006a), Climate sensitivity of moderate- and low-resolution versions of CCSM3 to preindustrial forcings, *J. Clim.*, *19*(11), 2567–2583.

Otto-Bliesner, B. L., E. C. Brady, G. Clauzet, R. Tomas, S. Levis, and Z. Kothavala (2006b), Last Glacial Maximum and Holocene climate in CCSM3, *J. Clim.*, *19*, 2526–2544.

Palais, J. M., M. S. Germani, and G. A. Zielinski (1992), Interhemispheric transport of volcanic ash from a 1259 AD volcanic-eruption to the Greenland and Antarctic Ice Sheets, *Geophys. Res. Lett.*, *19*(8), 801–804.

Pinto, J. P., R. Turco, and O. Toon (1989), Self-limiting physical and chemical effects in volcanic eruption clouds, *J. Geophys. Res.*, *94*(D8), 11,165–11,174.

Rasch, P. J., P. J. Crutzen, and D. B. Coleman (2008), Exploring the geoengineering of climate using stratospheric sulfate aerosols: The role of particle size, *Geophys. Res. Lett.*, *35*, L02809, doi:10.1029/2007GL032179.

Richter, J. H, F. Sassi, R. R. Garcia, K. Matthes, and C. A. Fischer (2008), Dynamics of the middle atmosphere as simulated by the Whole Atmosphere Community Climate Model, version 3 (WACCM3), *J. Geophys. Res.*, *113*, D08101, doi:10.1029/2007JD009269.

Rigor, I. G., J. M. Wallace, and R. L. Colony (2002), Response of sea ice to the Arctic oscillation, *J. Clim.*, *15*(18), 2648–2663.

Robock, A. (2000), Volcanic eruptions and climate, *Rev. Geophys.*, *38*(2), 191–219.

Robock, A. (2005), Cooling following large volcanic eruptions corrected for the effect of diffuse radiation on tree rings, *Geophys. Res. Lett.*, *32*, L06702, doi:10.1029/2004GL022116.

Robock, A., and Y. Liu (1994), The volcanic signal in Goddard-Institute-For-Space-Studies—3-dimensional model simulations, *J. Clim.*, *7*(1), 44–55.

Robock, A., L. Oman, and G. L. Stenchikov (2008), Regional climate responses to geoengineering with tropical and Arctic SO_2 injections, *J. Geophys. Res.*, *113*, D16101, doi:10.1029/2008JD010050.

Santer, B. D., et al. (2003), Contributions of anthropogenic and natural forcing to recent tropopause height changes, *Science*, *301*(5632), 479–483.

Shindell, D. T., G. A. Schmidt, R. L. Miller, and D. Rind (2001), Northern Hemisphere winter climate response to greenhouse gas, ozone, solar, and volcanic forcing, *J. Geophys. Res.*, *106*(D7), 7193–7210.

Shindell, D. T., G. A. Schmidt, R. L. Miller, and M. E. Mann (2003), Volcanic and solar forcing of climate change during the preindustrial era, *J. Clim.*, *16*(24), 4094–4107.

Shindell, D. T., G. A. Schmidt, M. E. Mann, and G. Faluvegi (2004), Dynamic winter climate response to large tropical volcanic eruptions since 1600, *J. Geophys. Res.*, *109*, D05104, doi:10.1029/2003JD004151.

Solomon, S. (1999), Stratospheric ozone depletion: A review of concepts and history, *Revs. Geophys.*, *37*(3), 275–316.

Stenchikov, G. L., I. Kirchner, A. Robock, H. F. Graf, J. C. Antuña, R. G. Grainger, A. Lambert, and L. Thomason (1998), Radiative forcing from the 1991 Mount Pinatubo volcanic eruption, *J. Geophys. Res.*, *103*(D12), 13,837–13,857.

Stenchikov, G., A. Robock, V. Ramaswamy, M. D. Schwarzkopf, K. Hamilton, and S. Ramachandran (2002), Arctic Oscillation response to the 1991 Mount Pinatubo eruption: Effects of volcanic aerosols and ozone depletion, *J. Geophys. Res.*, *107*(D24), 4803, doi:10.1029/2002JD002090.

Stenchikov, G., K. Hamilton, A. Robock, V. Ramaswamy, and M. D. Schwarzkopf (2004), Arctic oscillation response to the 1991 Pinatubo eruption in the SKYHI general circulation model with a realistic quasi-biennial oscillation, *J. Geophys. Res.*, *109*, D03112, doi:10.1029/2003JD003699.

Stenchikov, G., K. Hamilton, R. J. Stouffer, A. Robock, V. Ramaswamy, B. Santer, and H. F. Graf (2006), Arctic Oscillation response to volcanic eruptions in the IPCC AR4 climate models, *J. Geophys. Res.*, *111*, D07107, doi:10.1029/2005JD006286.

Stothers, R. B. (1996), Major optical depth perturbations to the stratosphere from volcanic eruptions: Pyhreliometric period, 1881–1960, *J. Geophys. Res.*, *101*(D2), 3901–3920.

Stothers, R. B. (2000), Climatic and demographic consequences of the massive volcanic eruption of 1258, *Clim. Change*, *45*(2), 361–374.

Thompson, D. W. J., and J. M. Wallace (2000), Annular modes in the extratropical circulation: Part I. Month-to-month variability, *J. Clim.*, *13*(5), 1000–1016.

Tilmes, S., R. Muller, and R. Salawitch (2008), The sensitivity of polar ozone depletion to proposed geoengineering schemes, *Science*, *320*(5880), 1201–1204.

Trenberth, K. E., and A. Dai (2007), Effects of Mount Pinatubo volcanic eruption on the hydrological cycle as an analog of geoengineering, *Geophys. Res. Lett.*, *34*, L15702, doi:10.1029/2007GL030524.

Wanner, H., et al. (2008), Mid- to Late Holocene climate change: An overview, *Quat. Sci. Rev.*, *27*(19–20), 1791–1828, doi:10.1016/j.quascirev.2008.06.013.

Wigley, T. M. L. (2006), A combined mitigation, *Science*, *314*(5798), 452–454.

Wigley, T. M. L., C. M. Ammann, B. D. Santer, and S. C. B. Raper (2005), Effect of climate sensitivity on the response to volcanic forcing, *J. Geophys. Res.*, *110*, D09107, doi:10.1029/2004JD005557.

C. M. Ammann, B. L. Otto-Bliesner, and D. P. Schneider, Climate and Global Dynamics Division, National Center for Atmospheric Research, P.O. Box 3000, Boulder, CO 80307, USA. (dschneid@ucar.edu)

D. S. Kaufman, Department of Geology, Northern Arizona University, 625 S Knoles Drive, Flagstaff, AZ 86011-4099, USA.